Nafion® Effects on Oxygen Reduction Catalysis by Carbon Supported Transition Metal Macrocycles and Platinum

Journal:	*The Journal of Physical Chemistry*
Manuscript ID	Draft
Manuscript Type:	Article
Date Submitted by the Author:	n/a
Complete List of Authors:	Chlistunoff, Jerzy; Los Alamos National Laboratory, Materials Physics and Applications Division Sansiñena, Jose-Maria; LANL: Los Alamos National Laboratory, C-CDE: Chemical Diagnostics & Engineering

Nafion® Effects on Oxygen Reduction Catalysis by Carbon-Supported Transition Metal Macrocycles and Platinum.

Jerzy Chlistunoff and José-María Sansiñena*

Los Alamos National Laboratory

P.O. Box 1663, Los Alamos, NM 87545

e-mail: jerzy@lanl.gov

ABSTRACT

The catalyst utilization in polymer electrolyte fuel cells (PEFCs) is never complete as a result of catalyst particle agglomeration and electronic or ionic isolation. Nafion®, the polymer electrolyte used in PEFCs contributes to the problem, since ORR can occur exclusively at the interfaces between its hydrated hydrophilic domains and the catalyst, but not at the respective interface involving the polymer's hydrophobic backbone. The paper presents the results of a voltammetric and RRDE study of ORR catalyzed by Fe and Co porphyrins and phthaloyanines adsorbed on a high surface area carbon (Vulcan XC72) and by carbon supported Pt catalysts in presence of various quantities of Nafion®. The results demonstrate that Nafion® self-assembles on both pristine or catalyst decorated carbon nanoparticles, when its content in the catalyst ink exceeds some critical value compared to that of carbon. The phenomenon is responsible for the catalytic site blocking and ORR inhibition. The extent of the inhibition depends on the type and the amount of the catalyst on the carbon surface and the degree of carbon surface graphitization. The activity of Co and Fe porphyrins and phthalocyanines is suppressed by up to two orders of magnitude, whereas that of low Pt loading (4.8%) catalysts by up to one order of magnitude. The results are discussed in terms of the catalyst layer morphology and the active site structure and suggest that heat-treated Fe/N/C composites, some of the most promising non-precious ORR catalysts, may be exceptionally susceptible to the surface blocking by Nafion®.

KEYWORDS: self-assembly, graphitic, catalyst support, hydrophobicity, heat-treated catalysts

INTRODUCTION

Nafion® is a polymer electrolyte commonly used in proton exchange membrane fuel cells (PEMFCs). It has a hydrophobic perfluorinated aliphatic backbone, whereas its side chains are outfitted with strongly acidic sulfonic groups responsible for providing proton conductivity.[1] The polymer is used as both the membrane material as well as the binder for highly dispersed catalysts in the anode and cathode catalyst layers of PEMFCs. Like other ion exchange polymers, Nafion® is phase separated. The perfluorinated backbone forms hydrophobic, whereas the sulfonic groups hydrophilic domains. In their hydrated state, the hydrophilic domains are capable of conducting hydrated protons. In a PEMFC, they provide environment, where hydrogen oxidation reaction (HOR, fuel cell anode) and oxygen reduction reaction (ORR, fuel cell cathode) can occur in presence of the aforementioned catalysts. The latter are typically platinum nanoparticles supported on high surface area carbons. The phase separation of the ionomer enables the formation of a continuous network of ion conducting channels, but it also eliminates some catalyst particles from the participation in the electrode reactions, when they contact ionically non-conductive, *i.e.*, hydrophobic parts of the ionomer. The incomplete catalyst utilization can be expected just from the statistical distribution of the catalyst particles[2] and the respective domains in the polyelectrolyte and it is also documented in the literature.[2-6] The phenomenon is of a relatively lesser importance for the anode reaction (HOR), which does not require much Pt to be effectively catalyzed. However, it is a serious concern for the cathode process (ORR) due to the sluggishness of the reaction[7-8] and the limited and largely monopolized Pt resources. In consequence, an extensive research aimed at the development of novel cathode catalysts has been conducted. The effort is directed towards either lowering the Pt loading necessary for the effective catalysis or replacing Pt (or other precious metals) with new materials. Among the novel materials, the most promising are

pyrolyzed Fe/N/C composites.[7-9] Their active sites are believed to comprise of Fe centers coordinated by four co-planar pyridinic nitrogen atoms embedded in graphene planes and arranged like in phenanthroline molecules.[8-9] As the phenanthroline groups do not necessarily belong to a common graphene plane, the coordination of the iron centers is frequently referred to as Fe-N_{2+2}.[9] This structure is very similar to that in numerous macrocyclic complexes known to be catalytically active in ORR, such as iron or cobalt porphyrins, phthalocyanines, and corroles.[10-14] The similarity lies not only in the square planar N_4 coordination of the metal center but also in the aromatic π-electron environment surrounding it. The active centers in the Fe/N/C composites and Pt based catalysts are completely different and promote different ORR mechanisms.[8, 12, 15] However, in practical applications, the catalysts of both types have a common feature. They both use a highly dispersed carbon as the catalyst support, whether the active centers are embedded in the support (Fe/N/C composites) or belong to independent catalyst crystallites (Pt based catalysts) deposited on larger carbon particles.

Before any new catalyst is tested in an operating fuel cell, it undergoes an extensive evaluation using numerous characterization techniques, but most importantly an electrochemical characterization in aqueous acidic electrolytes ($HClO_4$ or H_2SO_4) employing a rotating disk (RDE) or rotating ring disk (RRDE) electrode. If properly executed, RDE (RRDE) measurements can determine the intrinsic activity of a catalyst and its selectivity for the desired four electron reaction. The preparations for a typical RDE experiment involve fabrication of a catalyst ink, *i.e.*, a suspension of the highly dispersed catalyst in a suitable solvent, deposition of a small ink quantity onto the (typically glassy carbon) disk of an RDE (RRDE) and evaporation of the ink. The resultant catalyst layer has to be uniform, not too thick and it has to completely cover the disk of the electrode. As the catalyst film quality strongly depends on the ink properties, the ink formulation

is of crucial importance.[16] The catalyst ink must be well dispersed and durable, *i.e.*, it should not settle or clump. Nafion® is frequently added to catalyst inks to improve the catalyst dispersion and the catalyst layer integrity.

In this manuscript we compare the effects of Nafion® on the ORR catalysis by Pt and Co and Fe porphyrins and phthalocyanines supported on high surface area carbons under RRDE conditions. We will demonstrate that Nafion® present in the catalyst inks inhibits ORR to a different extent depending on the catalyst type and its relative amount compared to that of the carbon support.

EXPERIMENTAL

The following macrocyclic complexes were obtained from Aldrich and used as received: Iron (III) tetraphenylporphyrin chloride (5,10,15,20-Tetraphenyl-21*H*,23*H*-porphine iron(III) chloride, >94%, hereafter called FeTPPCl), iron(III) phthalocyanine chloride (~95%, hereafter called FePCCl), iron(III) octaethylporphyrin chloride (2,3,7,8,12,13,17,18-octaethyl-21*H*,23*H*-porphine iron(III) chloride, hereafter called FeOEPCl), cobalt(II) phthalocyanine (97%, hereafter called CoPC), cobalt(II) tetramethoxyphenylporphyrin (5,10,15,20-tetrakis(4-methoxyphenyl)-21*H*,23*H*-porphine cobalt(II), 97%, hereafter called CoTMeOPP), cobalt(II) octaethylporphyrin (2,3,7,8,12,13,17,18-Octaethyl-21*H*,23*H*-porphine cobalt(II), hereafter called CoOEP), cobalt(II) tetraphenylporphyrin (5,10,15,20-Tetraphenyl-21*H*,23*H*-porphine cobalt(II), 85%, hereafter called CoTPP).

Anhydrous dichloromethane (DCM, ≥99.8% with 50-150 ppm amylene as stabilizer, Sigma Aldrich), Vulcan XC72, a high surface area (~240 m^2 g^{-1}) carbon (Cabot) were used as received.

All experiments were performed using 0.5 mol dm^{-3} H_2SO_4 at 25 °C as the background electrolyte. The electrolyte was prepared using a commercial sulfuric acid (Certified ACS Plus, Fisher Chemical) and Millipore® water.

Highly ordered pyrolitic graphite (HOPG) grade SPI-2 (7 mm x 7mm x 1 mm platelet, mosaic angle 0.8° ± 0.2°, the lateral grain size up to 0.5 - 1 mm) was obtained from SPI Supplies and used as received.

The working electrode in RRDE experiments was a Pine model AFE7R9GCPT electrode with a glassy carbon disk and a platinum ring. Its nominal collection efficiency of 37% was confirmed by independent measurements using potassium ferricyanide in potassium chloride electrolyte solutions. In some voltammetric experiments a 3mm glassy carbon disk electrode (Bioanalytical Systems) was used.

Voltammetric HOPG electrodes were prepared as follows. A round opening was made with a steel punch (4.76 mm diameter) in a piece of Kapton® tape glued to a flat and smooth nylon block. Nylon was found to have a suitable hardness to allow for only a shallow penetration by the punch, which guaranteed smooth edges of the opening created in the tape without making damage to the punch cutting edge. After the round cutout was removed from the tape with a sharp tool, the tape was partially lifted from the block to expose the opening. Subsequently, an HOPG platelet, freshly cleaved with a piece of Scotch® tape, was placed on the block under the opening in the tape. The Kapton® tape was then carefully moved back down to create a seal between the edges of the platelet and the tape. A clean glass slide was used to press the tape against the HOPG. The quality of the seal thus obtained was subsequently examined under a microscope. Once the satisfactory seal was obtained, a piece of flexible copper foil was placed on the opposite (fully exposed) side of the platelet and the whole assembly covered with another piece of Kapton® tape. During the

last step, a special care was taken to avoid trapping air between the two Kapton® layers. Finally, the tape was trimmed with a razor. The electrode obtained in such a way was around 1.5 cm wide with the exposed HOPG surface area of ~0.18 cm^2 and exhibited an excellent durability in aqueous sulfuric acid solutions.

The counter electrode in all experiments was a graphite rod, whereas the reference electrode was a hydrogen electrode utilizing 6% H_2 in Ar in equilibrium with Pt black coated platinum wire immersed in 0.5 mol dm^{-3} H_2SO_4. The equilibrium potential of the reference electrode at Los Alamos elevation (2100 m) is 39 mV positive than the potential of a reversible hydrogen electrode (RHE) in the respective solution at the sea level.

In all RRDE experiments, the first scan was cathodic and the final potential was equal to the initial potential irrespective of the number of individual scans performed. The experiments were performed using electrode rotation rates ≥ 400 rpm and a scan rate of 10 mV s^{-1}, which guaranteed undistorted convective diffusion transport of oxygen to the electrode surface. The ring potential was held at +1.24 V vs. RHE to assure transport controlled oxidation of hydrogen peroxide generated in ORR. The voltammograms were corrected for the respective background currents measured in oxygen free solutions under the identical conditions. The background corrected currents (i_{corr}) were subsequently used to calculate the respective kinetic currents (i_k) using standard mass transfer correction: $i_k = i_{corr}i_L/(i_L-i_{corr})$, where i_L stands for the limiting ORR current.

In order to accurately determine electrochemical surface properties of the catalysts deposited onto the RRDE, multi-cycle voltammograms in oxygen free atmosphere were recorded at significantly higher scan rates (100 – 1000 mV s^{-1}). The voltammograms (and the capacitive currents extracted from them) reported in the paper were obtained from the second voltammetric cycles, which were not affected by uncontrolled electrode hold at the open circuit potential.

Two extensively characterized[17-21] commercial Pt catalysts supported on Vulcan were used in the study: 20% Pt (BASF) and 4.8% Pt (TEC10V05E, Tanaka Kikinzoku Kogyo). The third studied Pt (4.8%) catalyst was supported on graphitized carbon. Its properties were not disclosed by the manufacturer. The necessary X-ray diffraction and BET measurements were performed by the authors of the paper. The respective numbers are 157 $m^2 g^{-1}$ for the BET surface area and 4.8 nm for the average Pt particle size as determined from the Sherrer equation.[22] For simplicity, the three Pt catalysts will be hereafter called Pt20V (20% BASF), Pt4.8V (4.8% Tanaka), and Pt4.8G (Pt on graphitized support), respectively.

The catalyst inks for macrocyclic ORR catalysts were prepared using the following procedure. Around 40 mg of Vulcan XC72 were mixed with a few milligrams of the desired macrocycle and 2 - 4 cm^3 of DCM and slowly sonicated to dryness. Afterwards, the dry residue was sonicated for around 1 hour with 8 cm^3 of isopropanol (IPA) and small quantities of 5% Nafion® solution (Ion Power, Inc.). The inks of Pt catalysts and of pure XC72 carbon were prepared by directly mixing the solids with IPA and Nafion® followed by sonication. The amount of 5% Nafion® solution used to prepare the catalyst inks varied from 0 to 2.7 μl per 1 mg of the carbon support and was found to be an important parameter determining the extent of ORR inhibition for various catalysts. The ratio of the volume (μl) of 5% Nafion® solution to the weight (mg) of carbon support used for the catalyst ink preparation will be denoted by R, where R = 1 corresponds to 1 μl of the 5 % Nafion® solution used for 1 mg of the carbon support, which is equivalent to 46.8 μg of pure Nafion® per 1 mg of the support. The inks of Pt catalysts were prepared in a similar way, *i.e.*, a catalyst sample of ~40 mg was dispersed by sonication in 8 cm^3 of IPA with small Nafion® addition. As with the non-precious catalysts, the Nafion® content in those inks is hereafter expressed by the parameter R, *i.e.*, the ratio of the volume of 5% Nafion® in microliters to the

mass of carbon support in milligrams. All inks were stored in tightly closed glass vials at room temperature.

A Pine Instruments bipotentiostat model AFCBP1 controlled by Aftermath software (Pine Instruments) was used for all rotating ring disk experiments. Unless otherwise stated, all experiments were performed for a constant total loading of 0.1 mg of the carbonaceous support, which corresponds to 0.4 mg_{carbon} cm_{disk}^{-2}. The deposition of the ink on the glassy carbon disk of the RRDE and its evaporation were monitored under a microscope.

RESULTS

1. The effect of Nafion on the electrochemical behavior of Vulcan XC72

With its high specific surface area of ~240 m^2 g^{-1}, Vulcan XC72 significantly contributes to the overall surface area of catalysts utilizing it as the support and its interactions with Nafion® may alter the way the polymer electrolyte interacts with the catalyst particles. Consequently, the first part of our research was devoted exclusively to Vulcan, which was the catalyst support in all but one (Pt4.8G) studied catalysts. Cyclic voltammetry was selected to monitor changes in the available surface area of Vulcan in presence of Nafion®. The method is capable of directly measuring the electrical double layer charging currents of a conductive material, which are proportional to the surface area of the material remaining in contact with the electrolyte. Cyclic voltammograms were recorded for Vulcan XC72 inks containing from 0 to 1.5 μl of 5% Nafion® per 1 mg of carbon ($0 \leq R \leq 1.5$) in deoxygenated H_2SO_4 solutions at various scan rates ranging from 100 mV s^{-1} (Fig. 1) to 1000 mV s^{-1}. The measured currents were proportional to the scan rate, *i.e.*, exhibited capacitive character, in the entire potential range applied (0.04 – 0.74 V *vs.* RHE). They were virtually independent of Nafion® concentration for the inks containing up to and

including 0.6 µl of 5% Nafion® per 1 mg of XC72 (R = 0.6). However, when the Nafion® to carbon ratio (R) increased to 0.9 and above (0.9 < R ≤ 1.5), the measured currents dropped to

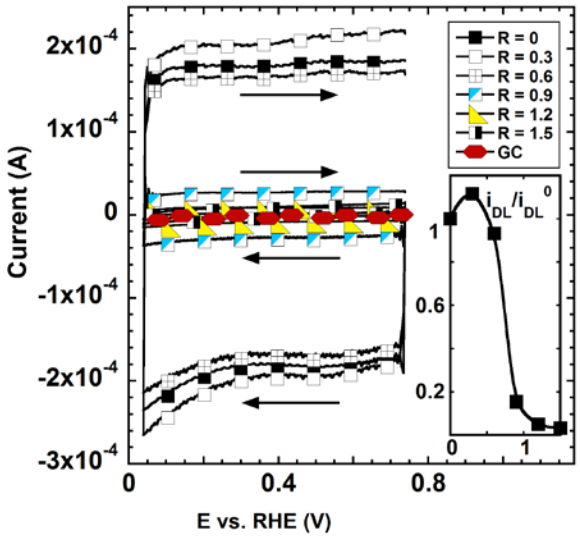

Figure 1. Capacitive voltammetric currents measured for 0.1 mg of Vulcan XC72 mixed with various quantities of 5% Nafion® solution. Scan rate 100 mV s^{-1}. R is the ratio of the volume of 5% Nafion® (µl) to the mass of carbon (mg) used to make the carbon inks. The ratio of the capacitive currents at 0.3 V for various Nafion® contents to that measured in absence of Nafion® is plotted against R in the inset. The currents used to create the graph in the inset were averages of the absolute currents measured at 0.3 V in both forward and reverse scans.

less than 20% and 10% of their initial values, respectively (Fig. 1). The suppressed currents still exhibited purely capacitive character. The changes in the capacitive currents demonstrate Nafion® adsorption on the carbon surface. The extent of the adsorption can be inferred from the measured double layer charging (capacitive) currents (i_{dl}). The charging current is proportional to the

differential (*i.e.*, potential dependent) double layer capacity of both Nafion® covered ($C_{dl,Nafion®}$) and free ($C_{dl,free}$) carbon surface:

$$i_{dl} = (C_{dl,free}(1-\Theta) + C_{dl,Nafion®}\Theta)A_{real}v \quad (1)$$

where A_{real} is the real surface area of the carbon deposited on the disk, v is the scan rate, whereas Θ is the surface coverage by Nafion®. Equation 1 neglects the contribution from the glassy carbon disk, whose surface area (~0.25 cm^2) is significantly lower than that of the XC72 (~240 cm^2 for the 0.1 mg loading). The equation can be used to calculate the surface coverages of the carbon surface by Nafion® for different Nafion® concentrations. In the calculations, the currents measured for the ink containing no Nafion® were identified with no surface coverage ($\Theta = 0$), whereas the currents measured for R = 1.5 were assumed to correspond to $\Theta = 1$ (maximum surface coverage) based on the observed flattening of the i_{dl} *vs*. R dependence at high Nafion® contents (inset in Fig. 1). The values of Θ obtained from eq. 1 were subsequently used to calculate the ratio of the surface area covered by Nafion® to the uncovered surface area ($\Theta/(1-\Theta)$). The resultant values were plotted *vs*. R to obtain the "adsorption isotherm" (Fig. 2). The real adsorption isotherm could not be determined, because the equilibrium concentrations of Nafion® in the inks corresponding to the measured surface coverage were unknown. They likely corresponded to unknown equilibrium states that were "frozen" at a later stage of the evaporation process due to the limited mobility of the large ionomer molecules between the already closely packed carbon particles. However, one can expect that the real adsorption isotherm would have a similar concave shape with even a steeper $\Theta/(1-\Theta)$ increase at high Nafion® concentrations. At R$\leq$ 0.6, virtually no adsorption is observed, *i.e.*, the equilibrium Nafion® concentrations corresponding to the

virtually zero surface coverages (and $\Theta/(1-\Theta)$) are unaffected and directly proportional to R in this concentration range. When significant adsorption starts taking place, the

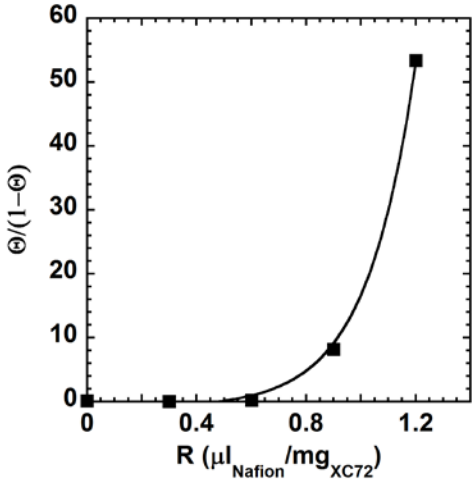

Figure 2. Calculated (eq. 1) ratio of surface areas of Vulcan XC72 covered with Nafion® and not covered plotted *versus* Nafion® content (R) in the ink.

R values are still unaffected, but the actual Nafion® concentration in solution is lowered by the adsorption. Consequently, the scale of the concentration axis will be contracted for $R > 0.6$ compared to the R scale and the respective increase in $\Theta/(1-\Theta)$ *vs*. concentration will be steeper than that in Fig. 2. The concave shape of the adsorption isotherm is consistent with the presence of strong attractive interactions in the adsorbed layer and implies a self-assembly character of the adsorption. In absence of such interactions, the adsorption would be described by Langmuir isotherm, which predicts a straight linear increase in $\Theta/(1-\Theta)$ with Nafion® concentration.[23] The lowest Nafion® concentration in IPA sufficient to promote the self-assembly of the ionomer on Vulcan is unknown. However, it can be estimated from a correlation between the observed ink dispersion behavior and the electrochemical data (Fig. 1). The inks with $R \leq 0.6$, whose

electrochemical behavior was virtually unaffected by Nafion® (Fig. 1), flocculated a short time after the sonication, irrespective of the sonication length. On the other hand, the inks with $R \geq 0.9$ were easily dispersed, stable almost indefinitely long and their respective double layer currents were significantly suppressed (Fig. 1). In those inks, Nafion® already acted as a surfactant protecting carbon particles from agglomeration. Hence, if the onset of Nafion® self-assembly is identified with $R = 0.9$, the respective minimum Nafion® concentration can be calculated as ~0.21 mg cm^{-3} for a 5 mg cm^{-3} suspension of XC72 in IPA.

As opposed to hydrophilic surfaces, which promote self-assembly of Nafion® through its hydrophilic (sulfonic) groups,[24] the self-assembly of Nafion® on XC72 occurs through the Nafion® hydrophobic component (perfluorinated backbone), as indicated by the magnitude of the observed suppression of the capacitive currents (Fig. 1). The suppression would not occur or was significantly smaller, if the ionically conductive component of Nafion® remained in contact with the carbon surface. Moreover, a self-assembly of Nafion® on Vulcan through the ionomer's hydrophilic component would not improve the dispersion of carbon particles in the hydrophilic solvent (IPA). On the other hand, the self-assembly involving the hydrophobic Nafion® component virtually eliminates the strong repulsive interactions between that component and the hydrophilic solvent through the hydrophobic interactions of the ionomer’s backbone with itself and with the carbon surface.

2. The effect of Nafion® on the electrochemical behavior of HOPG and GC

That the self-assembly of Nafion® on Vulcan occurs through the ionomer's hydrophobic component remains in agreement with the hydrophobic character of graphitic surfaces, which markedly contribute to the overall surface area of Vulcan.[25-26] In order to confirm the decisive role of graphitic surfaces in the self-assembly of Nafion® on Vulcan, a series of experiments were

performed with bare GC and HOPG electrodes in aqueous 0.5 M H_2SO_4 and mixed 35% (vol) isopropanol + 65% (vol) aqueous 0.5 M H_2SO_4 containing various quantities of either 5% Nafion® solution (sulfuric acid and IPA mixtures) or 50-fold diluted Nafion® solution in IPA (aqueous electrolyte). The experimental conditions were selected to mimic those encountered in the Vulcan inks. Contrary to our expectations, neither electrode material promoted self-assembly of Nafion® at the concentrations of up to 165 mg dm^{-3} (aqueous solutions) and 500 mg dm^{-3} (H_2O + IPA solutions), as demonstrated by the lack of meaningful changes of the respective capacitive currents during up to six hour periods following the ionomer additions. However, a clear difference between the affinities of Nafion® to disorganized (GC) and graphitic (HOPG) carbon surfaces was demonstrated for solution cast Nafion® films. The films were fabricated through the deposition of 10 μl aliquots of a Nafion® solution obtained by 50-fold dilution of the commercial (5%) Nafion® solution with isopropanol followed by a brief drying in air. While the presence of Nafion® film (confirmed both before and after the electrochemical experiments) had virtually no effect on the capacitive currents of GC, the surface of HOPG was found severely blocked (Fig. 3).

The effect of Nafion® on the electrical double layer of HOPG (Fig. 3) is consistent with Nafion® self-assembly[27] promoted by the attractive interactions between its hydrophobic component and the ordered and hydrophobic graphitic surfaces. In similarity to HOPG, carbon atoms in GC are also sp2 hybridized, but form a randomly distributed network of fullerene-like structures.[28] In consequence, a polished surface of the material is expected to exhibit an “amorphous” character and significantly lower hydrophobicity, which cannot promote strong interactions with the hydrophobic component of the ionomer. The structural differences between HOPG and GC confirm that the partially graphitic character of the Vulcan surface[26] plays a decisive role in the

self-assembly phenomena described in the previous section. The lack of Nafion® self-assembly on flat HOPG surfaces in presence of liquid (electrolyte) phase does not contradict the above

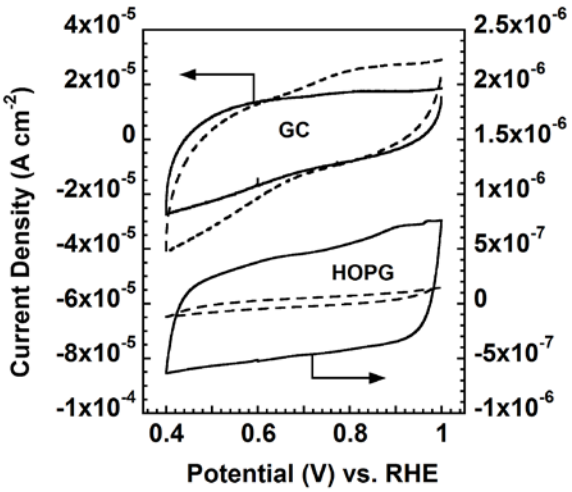

Figure 3. Capacitive voltammetric current densities measured for a 3 mm glassy carbon disk and a 4.8 mm HOPG electrode in 0.5 mol dm^{-3} sulfuric acid before (solid lines) and after depositing Nafion® film (see text). Scan rate 100 mV s^{-1}.

conclusion. As opposed to relatively small (~30 nm) Vulcan particles,[19] which can be virtually encircled by a single Nafion® strand interacting through its hydrophobic backbone with the carbon surface and itself, significant extent of Nafion® ordering is required on virtually atomically flat HOPG surfaces.[27] The respective entropy change is significantly less favorable than that associated with the Nafion® self-assembly on small carbon particles, which does not require a concerted alignment of multiple Nafion® molecules.[27] Instead, a single Nafion® strand, whose length can vary from ~200 nm to ~ 2000 nm as estimated from the reported average molecular weight of the polymer,[1] is sufficient to self-align around a ~30 nm Vulcan particle. The self-assembly of

Nafion® on small carbon particles may be additionally promoted by a favorable entropy contribution associated with the deagglomeration of the particles.

3. Nafion® effects on the kinetics of ORR catalyzed by Co and Fe macrocycles adsorbed on Vulcan XC72

In order to quantitatively evaluate Nafion® effects on ORR catalyzed by macrocyclic complexes, a model system meeting the specific requirements of high stability and well defined ORR mechanism had to be selected. All catalysts containing the macrocyclic complexes adsorbed on Vulcan XC72 dispersed with significant difficulty in pure IPA and even more so in water and

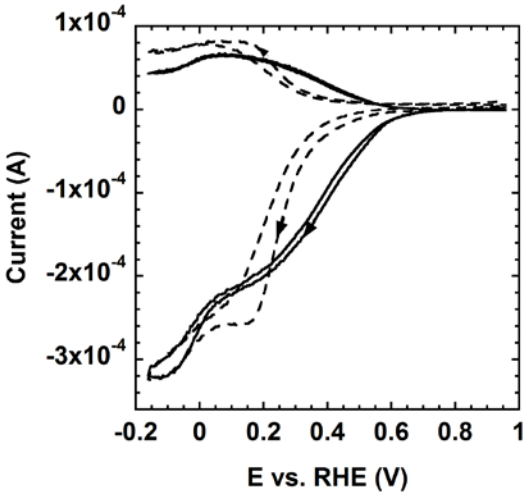

Figure 4. Background corrected RRDE currents for ORR (disk – negative, ring – positive) recorded for 7.5% CoPC supported on Vulcan XC72 and two Nafion® contents. R = 0.3 - solid lines, R = 1.2 – dashed lines. Total carbon loading 0.1 mg. Rotation rate 400 rpm. Scan rate 10 mV s^{-1}.

their inks easily flocculated afterwards. Addition of Nafion® to the inks facilitated the catalyst dispersion. The lowest amount of Nafion® that allowed for a barely acceptable quality of the

catalyst layer on the RRDE disk corresponded to R = 0.3. On the other hand, the inks with R = 1.2, which guaranteed almost full surface coverage of the carbon support by Nafion® (Fig. 1), did not flocculate and created uniform catalyst layers. The aforementioned selection of the model system was accomplished based on experiments performed for these two Nafion® contents.

The experiments revealed that the iron macrocycle based catalysts (FeTPPCl, FeOEPCl, and FePCCl) were quickly deteriorating during RRDE measurements. In multiple scan experiments, every single cycle was shifted cathodically from the previous one, irrespective of the Nafion® content. The rate of deterioration was changing in the following order: FePCCl > FeTPPCl ≥ FeTOEPCl. On the other hand, the catalysts containing Co based complexes, *i.e.*, CoPC, CoTMeOPP, CoOEP, and CoTPP produced more stable electrochemical behavior. For all Co based inks with R = 0.3, the forward (cathodic) scans of the background corrected RRDE voltammograms were virtually identical with the reverse (anodic) ones, indicative of a mixed kinetic/transport control of the reaction. The measured currents were practically independent of the number (up to ten) of cycles. For the same catalysts with R = 1.2, the background corrected oxygen reduction currents in the kinetic region of the forward (cathodic) scans were higher than those in the reverse scans (Fig. 4), but the catalysts were stable, *i.e.*, virtually identical voltammograms were recorded irrespective of the number of cycles in the voltammetry. We found that surface confinement of oxygen was responsible for the higher ORR currents in the forward scans. The phenomenon was also detected for Fe based catalysts with R = 1.2, but it was obscured by the progressive catalyst degradation. Our subsequent paper will deal with the oxygen confinement in great detail. For the present study, it is essential that the currents in the reverse (anodic) scans were not affected by the phenomenon and determined exclusively by electrochemical kinetics and oxygen transport. Consequently, all kinetic data presented below for

the ORR catalyzed by the macrocyclic complexes were obtained from the respective reverse (anodic) scans.

Except for CoPC (Fig 4), the ORR catalyzed by all studied macrocycles under RRDE conditions produced a single reduction wave at both R = 0.3 and R = 1.2. However, the number of electrons in ORR was noticeably increasing with the overpotential for these complexes, whereas it was practically constant and very close to 2 for the major wave in ORR voltammograms recorded for CoPC (Fig 4), which indicated that hydrogen peroxide was the main oxygen reduction product for that complex. The reaction stoichiometry for CoPC was also virtually unaffected by the quantity of Nafion® in the ink, whereas the relative contribution of the two-electron reaction was significantly higher at R = 1.2 than at R = 0.3 for the remaining complexes (Table 1). A single rotation rate of 400 rpm was selected for the kinetic analysis of the ORR catalyzed by the macrocyclic complexes. This rotation rate guaranteed the highest accuracy of the measurement of the transport controlled currents, which was required for the kinetic current determinations. Higher rotation rates, especially for R = 1.2, frequently resulted in not well defined limiting currents due

Table 1. Number of electrons[a)] transferred in ORR catalyzed by cobalt and iron porphyrins and phthalocyanines.

Catalyst	n at R=0.3	n at R =1.2
CoPC[b)]	2.05 - 2.34	2.20 - 2.37
CoOEP	2.84 - 3.56	2.05 - 2.36
CoTPP	2.62 - 3.12	2.27 -2.40
CoTMEOP	3.10 - 3.24	2.40 - 2.65
FeTPPCl	2.10 - 3.90	2.40 - 3.95
FeOEPCl	2.40 - 3.92	2.20 - 3.80
FePCCl	2.10 - 3.90	3.00 - 3.28

[a)]The numbers show the range of n measured over the respective potential range corresponding to the kinetic currents shown in Fig. 4

[b)]The major reduction wave (Fig. 3)

to a partial overlap of the currents originating from the ORR and the electrolyte decomposition.

Figure 5 shows the kinetic, *i.e.*, transport corrected ORR currents recorded for all studied macrocycles and two Nafion® contents (R = 0.3 and R = 1.2) in the catalyst inks. Very significant cathodic shifts are

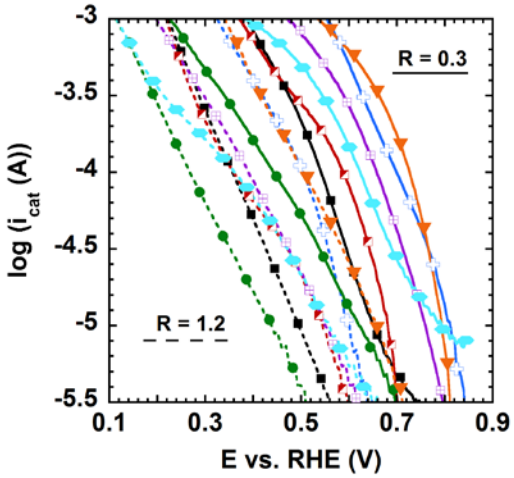

Figure 5. Kinetic ORR currents determined from first reverse (anodic) scans of RRDE voltammograms measured for Co and Fe porphyrins and phtalocyanines supported on Vulcan XC72. Nafion® content (R): 0.3 – solid lines, 1.2 – dashed lines. Total Vulcan XC72 loading 0.1 mg. Rotation rate 400 rpm. Scan rate 10 mV s^{-1}. Weight percentage of the complexes in the catalysts (excluding Nafion®): FeOEPCl – 8.1 (full black squares); FeTPPCl – 9.0 (half filled red squares); CoOEP – 7.6 (blue crosses); CoPC – 7.5 (full green circles); CoTPP – 8.6 (purple crossed squares); CoTMeOPP – 6.2 (orange triangles); FePCCl – 7.9 (light blue hexagons).

observed for all inks with R = 1.2. The magnitude of the shift was similar for most macrocycles and varied between ~200 mV and ~300 mV with the ORR overpotential. For CoPC and FeOEPCl, the potential shifts did not exceed 200 mV. In close similarity with the Nafion® effects on the

capacitive currents measured for XC72 (Fig. 1), the background currents (not shown) measured for the inks with R = 1.2 were also significantly lower than those recorded for the inks with R = 0.3. As demonstrated by the above data, the strong detrimental effect of Nafion® on the ORR catalysis by the Vulcan supported macrocyclic complexes is not selective. Consequently, similar effects of Nafion® on other carbon supported catalysts can be expected.

The Nafion® and potential induced changes in the number of electrons involved in ORR and the inaccuracies in the determination of the respective limiting currents made us abandon Koutecky-Levich[29] analysis for the majority of the studied complexes. The analysis was performed exclusively for CoPC, whose electrochemical behavior in ORR was relatively well defined. While the partial overlap between the first oxygen reduction wave and the ill-defined second one compromised the quality of the Koutecky-Levich analysis of the first wave, the results demonstrated that the Nafion® layer had virtually no effect on oxygen transport to the catalytically active sites. These data will be shown together with the respective Koutecky-Levich plots determined for the Pt catalysts (Fig. 12). Due to its stable and relatively better defined electrochemical behavior in ORR (Table 1) CoPC was also selected for further kinetic studies.

4. Nafion® effects on the kinetics of ORR catalyzed by CoPC – ionomer and macrocycle loading effects.

The low Nafion® quantity (R = 0.3) used in some of the previous experiments (Fig. 5) did not guarantee sufficiently good quality of the respective catalyst layers. Consequently, the smallest amount of Nafion® used for the studies described in this section corresponded to R = 0.6. Such amount of Nafion® resulted in somewhat better catalyst film quality without a significant ORR inhibition.

Inks containing three different CoPC quantities (1.7% (w/w), 5.7% (w/w), and 13.6% (w/w)) and variable quantity of Nafion® ($0.6 \leq R \leq 2.4$) were prepared. The quantities of CoPC in the three inks corresponded to ~100%, 350% and 910% of the full surface coverage, assuming CoPC molecules adsorbed flat on the entire carbon surface.[30] If only basal (graphitic) carbon planes supported the phthalocyanine,[31] there would be an excess of the compound for all three catalyst compositions. In either case, if CoPC molecules adsorbed flat and did not agglomerate on the carbon surface, all three catalyst compositions would produce the highest possible surface coverage by CoPc molecules with the excess of CoPC forming nonconductive and thus inactive crystals. Indeed, small shiny crystallites of the phthalocyanine were clearly visible under a microscope during the evaporation of the 5.7% and 13.6% inks containing 0.6 μl of 5% Nafion® solution per 1 mg of the carbon support (R = 0.6). While the crystallites were also visible for higher Nafion® contents, their number seemed to decrease with R and virtually none of them could be observed for $R \geq 1.5$. Spectrophotometric measurements with CoPC suspensions in mixed IPA + Nafion® solutions revealed that Nafion® had no effect on CoPC solubility in the inks. Therefore, it was reasonable to assume that CoPC crystallites were present in the inks irrespective of the Nafion® content, but their view became progressively obstructed by better dispersed carbon particles in the inks with higher Nafion® concentrations.

4.1. CoPC loading effect (R = 0.6).

In agreement with the expected CoPC surface saturation, the activities of the catalysts containing 1.7% and 5.7% CoPC were comparable (Fig. 6). However, the catalyst containing 13.6% CoPC was found more active (Fig. 6). Its higher activity resulted from a higher number of electrochemically active CoPC molecules on the surface as manifested by the better defined CoPC reduction/reoxidation peaks (at ~0.7 V and ~0 V) in the respective voltammograms recorded for

that catalyst in oxygen free atmosphere (inset Fig. 6). The faster ORR kinetics was not accompanied by a change in the reaction mechanism, *i.e.*, the number of electrons in ORR stayed virtually identical to that observed for the other two catalysts (see the legend of Fig. 6). The higher apparent surface density of the active sites in the 13.6% catalyst may result from a partial overlap between the adsorbed CoPC molecules (*i.e.*, a higher loading than that corresponding to the close packed monolayer) and/or a large number of CoPC crystallites present in the catalyst layer. The latter may act as nonconductive spacers, which reduce the agglomeration of the carbon support particles likely occurring through the strongly hydrophobic phthalocyanine molecules. In

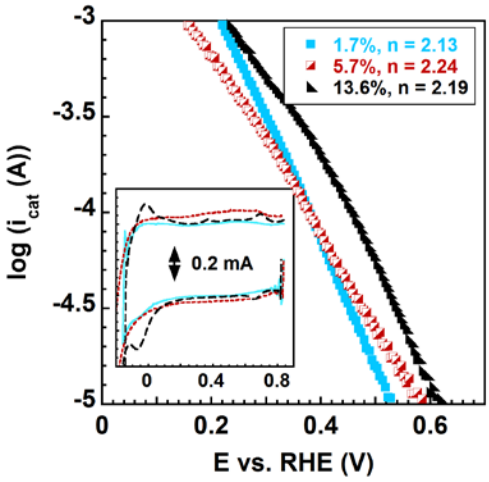

Figure 6. Kinetic ORR currents determined from first reverse (anodic) scans of RRDE voltammograms measured for various quantities of CoPC supported on Vulcan XC72. R = 0.6. Total carbon loading 0.1 mg. CoPC contents (weight %) listed in the legend. Rotation rate 400 rpm. Scan rate 10 mV s^{-1}. Inset: cyclic voltammograms recorded for the catalysts in absence of oxygen at 100 mV s^{-1}. CoPC contents (weight %): 1.7 – solid blue line; 5.7 – short dashed red line, 13.6 – long dashed black line. Reduction and oxidation peaks corresponding to CoPC are clearly visible only for the 13.6% CoPC (long dashed black line).

consequence, a higher number of the active sites adsorbed on the surface of the carbon support may be exposed and participate in ORR. Further insight into the potential causes of the higher activity of the 13.6% catalyst will be presented in the following section.

4.2. *Nafion® concentration effects*

Figure 7 demonstrates the effects of increasing quantity of Nafion® on the catalytic activity for ORR of the catalysts containing 1.7%, 5.7% and 13.6% CoPC. The reaction on all catalysts becomes strongly

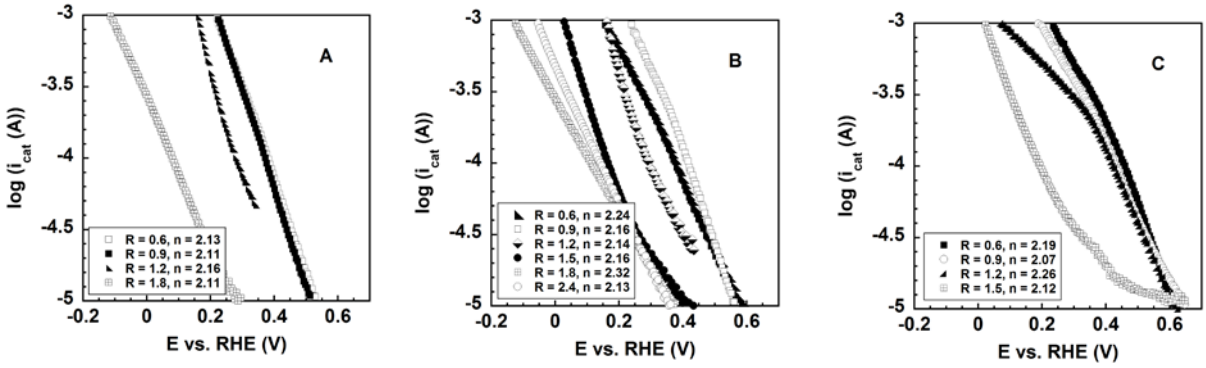

Figure 7. Effects of Nafion® on the kinetic ORR currents for catalysts containing three different quantities of CoPC: 1.7% (A); 5.7% (B); 13.6% (C). Total Vulcan XC72 loading 0.1 mg. Rotation rate 400 rpm. Scan rate 10 mV s^{-1}. Nafion contents (R) and average number of electrons transferred in ORR (n) listed in the legend.

inhibited, when Nafion® concentration in the catalyst increases. The observed reduction potentials shift cathodically by as much as 300 mV, when the Nafion® content increases from R = 0.6 to R = 1.8.

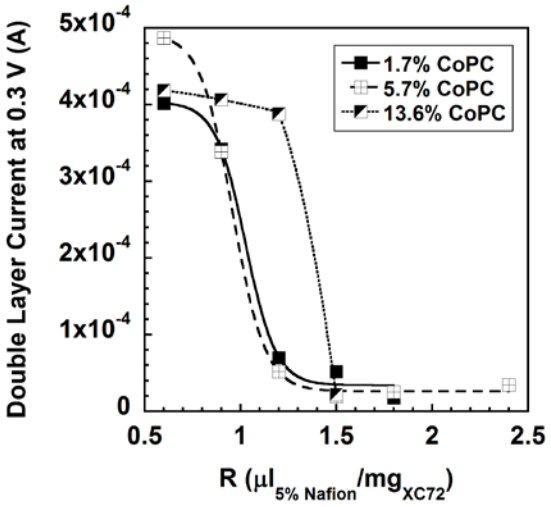

Figure 8. Capacitive currents at 0.3 V for three CoPC + XC72 catalysts plotted against the Nafion® content (R) in the ink. The values plotted are sums of the absolute currents measured in both forward and reverse voltammetric scans recorded at a scan rate of 100 mV s^{-1}. Total Vulcan XC72 loading 0.1 mg.

The changes in ORR kinetics for all three catalysts do not have a continuous character but occur rather stepwise within the narrow concentration range of Nafion®. The kinetic changes are not accompanied by any changes in the reaction selectivity for hydrogen peroxide (number of electrons in ORR listed in the figure). The catalysts containing 1.7% and 5.7% CoPC behave similarly in that a change in the reaction kinetics is already advanced at R = 1.2. For the catalyst containing 13.6 % CoPC, the major kinetic change occurs after R reached 1.2. A similar "delay" is also visible in the graph showing the suppression of the respective capacitive currents by Nafion® adsorption (Fig. 8). This behavior may have its origin in the already postulated effect of CoPC crystallites acting as carbon particle separators, which make a larger fraction of the carbon surface available

for ORR but also for Nafion® adsorption. Moreover, the crystallites can compete with carbon particles as the hydrophobic centers for the self-assembly of Nafion®.

A series of experiments (not shown) was also performed with CoPC catalyst films (5.4% CoPC), where various quantities of a diluted Nafion® solution (1 cm^3 of 5% Nafion® diluted 100-fold in deionized water) were deposited on top of the catalyst films containing no Nafion®. In agreement with the self-assembly hypothesis, the ionomer introduced to the catalyst layer in this way had virtually no effect on either background currents or ORR kinetics even if the nominal content of Nafion® in the catalyst layer corresponded to R as high as 5 (234 μg of pure Nafion® per 1 mg of XC72).

5. The effect of Nafion® on ORR catalyzed by carbon supported platinum

The effects of Nafion® on ORR catalyzed by platinum were studied for three catalysts containing from 4.8% Pt to 20% Pt. The catalyst with the highest Pt content (20% Pt on XC72) was found to be virtually unaffected by Nafion® up to and including R = 2.7. Neither the cyclic voltammograms recorded for the catalyst in absence of oxygen nor the RRDE voltammograms recorded for oxygenated solutions were visibly changing within the specified range of Nafion® concentration in the catalyst ink. The same was true for the number of electrons transferred in ORR, which did not deviate from 4 by more than 0.02 under all studied conditions. In Fig. 9A are shown the respective voltammograms recorded for the catalyst in deoxygenated solutions. All, the hydrogen underpotential deposition (H_{UPD}) (E < 0.4 V), platinum oxide formation (E > 0.8 V), and platinum oxide reduction (E < 1.0 V) regions in the voltammograms are well defined and practically insensitive to the Nafion® content. As the oxide formation and reduction processes occur with overvoltages, the ORR kinetics is slower, when the electrode potential is scanned

cathodically, as it starts when the Pt surface is partially covered with Pt oxide[32]. Consequently, in Fig. 9B are shown the respective Tafel plots obtained from the data collected

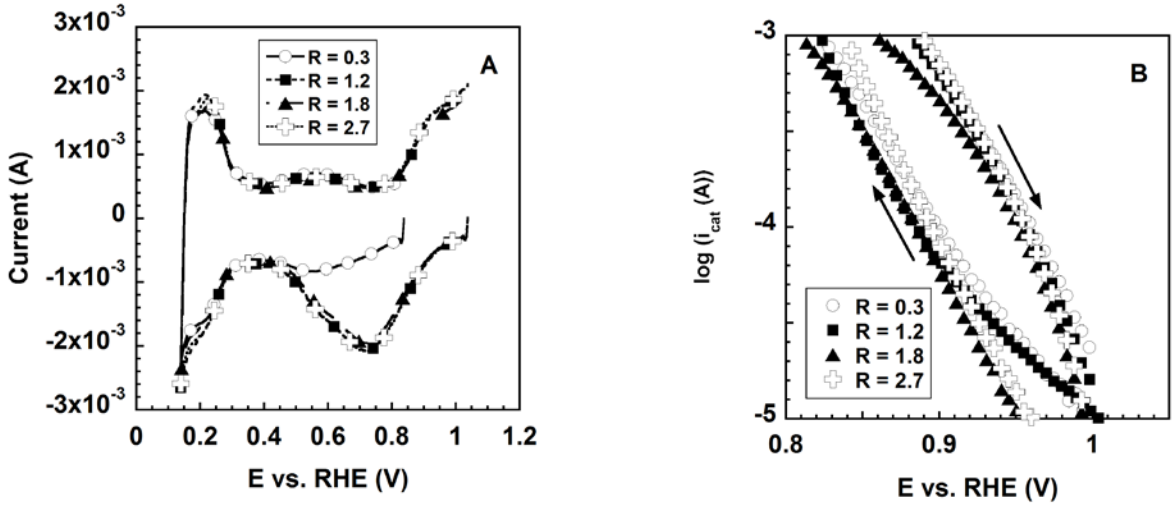

Figure 9. Background currents (A) and ORR kinetic currents (B) measured for Pt20V (0.1 mg total carbon loading) containing various Nafion® quantities (R). Scan rate: 100 mV s^{-1} (A); 10 mV s^{-1} (B). Rotation rate (B): 400 rpm. Scan directions (B) indicated by the arrows parallel to the Tafel plots.

during both forward (cathodic) and backward (anodic) potential scans in the RRDE experiments. Somewhat slower ORR kinetics can be observed for the partially oxidized Pt surfaces (forward scans) of the inks containing higher quantities of Nafion® (R = 1.8 and R = 2.7). A slower ORR kinetics is also visible in the reverse scan recorded for the catalyst ink with R = 1.8. Since the respective background currents were virtually identical for all Nafion® contents (Fig. 9A), we believe that the observed kinetic differences for the catalyst are likely associated with inadequate background correction at low and high overvoltages, where the ORR currents are either very low or very close to the limiting currents and the standard mass transfer correction is least accurate.

In spite of the identical Pt content (4.8%) in the two low Pt loading catalysts, there were measurable differences in their electrochemistry (Fig. 10). The catalyst supported on graphitized carbon (Pt4.8G) exhibited generally lower background currents in the whole studied potential range, *i.e.*, in the hydrogen UPD (H_{UPD}), PtO formation/reduction and the double layer (determined predominantly by the carbon support) regions. This was true for all Nafion® concentrations in the inks (Fig. 10).

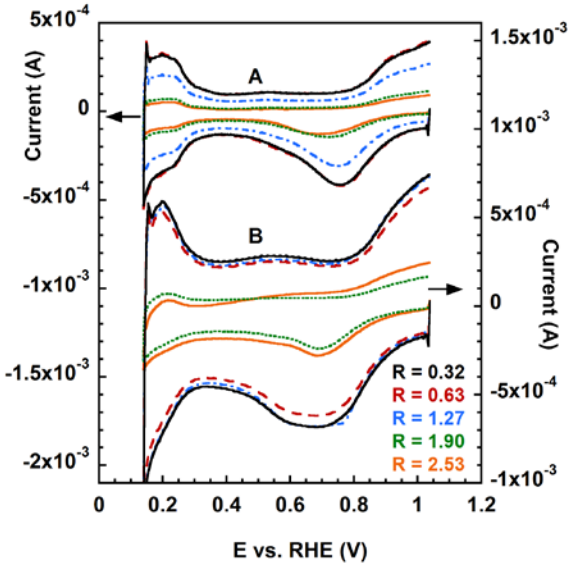

Figure 10. Background currents measured for Pt4.8G (A) and Pt4.8V (B) catalysts containing various quantities (R) of Nafion®. Scan rate 100 mV s^{-1}. Total carbon support loading 0.1 mg.

The lower double layer currents for Pt4.8G have the origin in the more graphitic character of its carbon support (Fig. 3) and its lower specific surface area (156 m^2 g^{-1} for the catalyst) compared to that of Vulcan in Pt4.8V (~240 m^2 g^{-1}). Lower H_{UPD} and Pt oxide currents measured for Pt4.8G are expected from its larger Pt particle size (4.8 nm) compared to that of Pt4.8V (number averaged 2.2 nm, surface averaged 2.6 nm[18]). The difference is better reflected in the respective Pt oxidation

and oxide reduction currents than in H_{UPD}, which is not completely covered in the potential range selected for the measurements in Fig. 10.

Both low Pt loading catalysts were affected by increased Nafion® concentration (R) in a way qualitatively similar (Figs. 10 and 11) to that observed for the organic macrocycles.

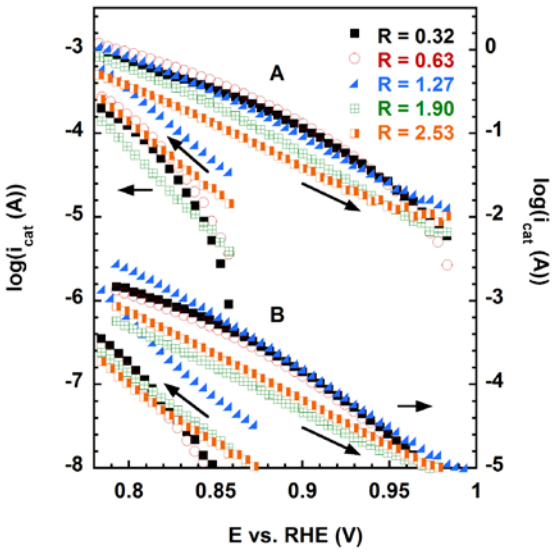

Figure 11. ORR kinetic currents measured for Pt4.8G (A) and Pt4.8V (B) catalysts containing various quantities (R) of Nafion®. Scan rate 10 mV s^{-1}. Rotation rate 400 rpm. Scan directions indicated by the arrows parallel to the Tafel plots.

The background currents in the whole potential range dropped virtually stepwise with an increase in the Nafion® content in the ink demonstrating that both carbon and Pt surfaces were blocked by the ionomer. As expected, the respective ORR currents (especially in the anodic scan, *i.e.*, for the reduced Pt surface) were also suppressed, but the kinetic changes were not accompanied by any change in the virtually 100% reaction selectivity for water. The largest negative departure from 4 of the number of electrons involved in ORR was 0.05 for the Pt4.8V catalyst at R = 1.90. The lack of substantial changes in the reaction selectivity demonstrates that

the Pt surface blocking did not involve individual Pt active centers but large fractions of the Pt surface area. The surface blocking and the kinetic effects were notably smaller for the low loading Pt catalysts than those observed for the macrocyclic catalysts. The background currents dropped by a factor of no more than 3.5. The oxygen reduction potentials on the oxide free Pt surface (anodic scans) were shifted by up to 60 mV, which corresponds to a ~3-fold decrease in the kinetic current. However, the effects of Nafion® on both low Pt loading catalysts were not identical and small quantitative differences between those effects could be seen. The first noticeable loss of the electrochemically accessible surface area for the catalyst with the graphitized support (Pt4.8G) occurred between R = 0.63 and R = 1.27, whereas no surface losses could be observed for the catalyst with standard Vulcan support (Pt4.8V) before R reached 1.27 (Fig. 10). This finding remains in agreement with the tendency of Nafion® to self-assemble on graphitic surfaces, demonstrated in this paper and elsewhere[27, 33] and the more graphitic character of the carbon surface in Pt4.8G. The respective changes in ORR kinetics (Fig. 11) did not follow exactly the same pattern. For Pt4.8G, the kinetic ORR currents in the anodic scans (reduced Pt surface) were lowest for the ink containing the highest Nafion® quantity (R = 2.53), whereas the slowest ORR kinetics for the Pt4.8V was observed at R = 1.9. The difference most likely reflects the effects of carbon surface properties on the distribution of Pt particles.[34] The kinetic currents measured for the Pt surfaces partially covered with Pt oxide (cathodic scans) were much less sensitive to the Nafion® content except for the ink composition corresponding to R = 1.27. Unexpectedly, the ORR currents measured for both low Pt loading catalysts in the forward scan were up to three times higher for this particular composition than for all other compositions corresponding to both higher and lower Nafion® contents. The departures of the kinetic ORR currents from the expected inverse proportionality between them and the measured background currents for the two low Pt

loading catalysts may have resulted from differences in the experimental conditions applied in the respective experiments. The background currents were recorded using a scan rate of 100 mV s^{-1} (Fig. 10), whereas the kinetic currents were obtained from RRDE experiments employing a scan rate of 10 mV s^{-1} (Fig. 11). The latter may have enabled structural changes in the Nafion® layer[35] during the time consuming RRDE experiments. As opposed to CoPC, oxidized Pt is hydrophilic and its potential dependent surface may create conditions suitable for such changes.

6. Nafion® effects on oxygen transport to catalytically active sites

In Fig. 12 are shown the intercepts of the Koutecky-Levich plots obtained for the limiting oxygen reduction currents recorded for the two low Pt loading catalysts (Pt4.8V and Pt4.8G) and a 4.2% CoPC adsorbed on Vulcan XC72. As opposed to the measured ORR kinetics, the oxygen transport to catalyst particles in the two Pt catalysts is not affected by the self-assembly of

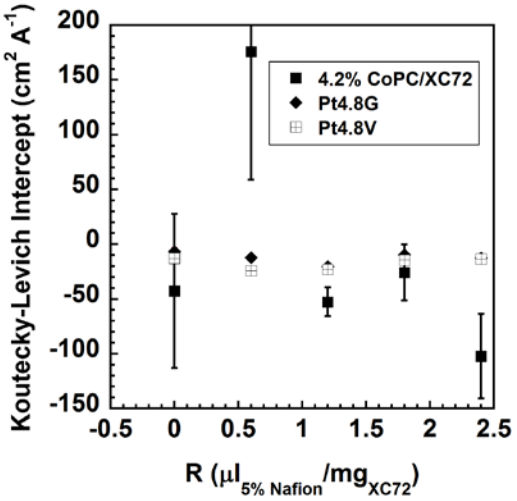

Figure 12. Intercepts of the Koutecky-Levich plots for the limiting ORR currents in O_2 saturated solutions measured from experiments performed at 400, 625, 900, 1225, 1600, 2025 and 2500 rpm rotation rates. The error bars reflect the respective errors of the intercepts obtained from the linear fitting and are too short to be seen for the Pt catalysts.

Nafion®. This fact combined with the lack of Nafion® effect on the ORR selectivity demonstrates that Nafion® blocks either entire Pt particles or the continuous fractions of their facets and the blocked surfaces do not participate in ORR at all. Therefore, the ORR inhibition results entirely from a loss in Pt surface area due to its ionic isolation by the hydrophobic component of the ionomer. While the Koutecky-Levich intercepts for the CoPC catalyst are disturbed by quite significant errors, they oscillate around zero and do not exhibit any meaningful trend.

This indicates that the Nafion® films do not block oxygen transport to the active CoPC particles. Consequently, the latter must be located either in small openings between Nafion® strands or in larger areas which remained unoccupied by Nafion® due to either steric barriers or an overall higher surface hydrophilicity (non-basal planes).

DISCUSSION AND CONCLUSIONS

The results presented in the previous sections demonstrate a significant affinity of Nafion® to pure Vulcan XC72, all non-precious macrocyclic complexes adsorbed on XC72 and low Pt content (4.8%) carbon supported catalysts but not to 20% Pt/Vulcan XC72. These observations demonstrate that the self-assembly of Nafion® on the catalysts is predominantly determined by the carbon support, but it is also influenced by the number, size and surface properties of the catalyst particles. The present data also show that the extent of ORR inhibition is different for different types of catalysts. The self-assembled layers of Nafion® led to a decrease of the kinetic ORR currents on the transition metal catalysts by up to two orders of magnitude, whereas the kinetics of ORR on the two low Pt loading (4.8%) catalysts decreased under similar conditions by less than one order of magnitude (Fig. 11). The differences in ORR inhibition between the Pt catalysts and the macrocyclic catalysts reflect the differences in their morphology. The iron and cobalt macrocycles are electrocatalytically active only as single or at most weakly agglomerated

molecules, since their respective crystals are nonconductive. The molecules of the macrocyclic catalysts possess highly delocalized π-electron clouds responsible for their hydrophobicity and the strong attractive interactions with the hydrophobic carbon surface, especially with its graphitic planes.[31] These interactions promote a flat orientation of the macrocycles on the surface. Due to the flat orientation of the hydrophobic catalytic molecules on the hydrophobic surface, neither the surface hydrophobicity nor its morphology is significantly affected. In consequence, the Nafion® hydrophobic component can easily adsorb on both bare and catalyst coated carbon surfaces. The adsorbed macrocyclic complexes can participate in ORR only when they are not completely blocked by the hydrophobic backbone of Nafion®. In order for this to happen, they must be located below small openings between the adsorbed ionomer chains, which allow for the access of oxygen, water and H^+ to the active sites. As there exist strong attractive interactions between the ionomer chains in the adsorbed layer, it is not difficult to imagine that only a small fraction of the catalytically active molecules can participate in ORR. The approximately two order of magnitude decrease in ORR kinetics resulting from Nafion® adsorption on the CoPC catalysts (Fig. 8) indicates that only 1% of the active centers retain their ability to reduce oxygen under such conditions.

The situation is significantly different for the Pt catalysts. The preferred orientation of Nafion® molecules in contact with an oxidized Pt is that with its hydrophilic component facing the hydrophilic oxidized surface. In presence of liquid water (electrolyte), Nafion® maintains an open morphology at its interface with bare Pt surface,[36] even if its hydrophobic component previously occupied that interface in absence of liquid water.[35] Moreover, as oxygen was not eliminated during the preparation of the Pt catalyst inks, the surface of Pt particles was at last partially oxidized and thus hydrophilic. Therefore, no Pt surface blocking is expected for carbon supported

Pt catalysts under RRDE conditions unless the hydrophobic interactions between the catalyst support and Nafion® backbone are strong enough to impose the same Nafion® orientation over the neighboring Pt particles. This does not happen for Pt20V, where ~30 nm[19] Vulcan particles support ~2.1 nm[20] Pt nanocrystals, whose centers are on average only ~9 nm apart assuming a uniform hexagonal Pt particle distribution on the outer surface of the carbon particle. However, the estimated average distance of ~22 nm between ~2.2 nm Pt particles on Vulcan in Pt4.8V[18] is sufficiently large to allow for the self-assembly of the ionomer on the support and its subsequent spillover onto the Pt particles. The slightly stronger inhibiting effect of Nafion® on ORR catalyzed by Pt4.8G than that observed for Pt4.8V results from the combination of a number of factors. The more graphitic surface character of the support in Pt4.8G, which results in stronger attractive carbon-Nafion® interactions (Fig. 10) is likely the most important factor responsible for the observed difference. The relative roles of the differences in actual Pt surface areas (Fig. 10), carbon and Pt particle sizes and the uniformity/non-uniformity of Pt particle distribution[34] in both low Pt loading catalysts are more difficult to quantify. However, the potential steric factors resulting from the larger size (4.8 nm) of Pt particles in Pt4.8G compared to that in Pt4.8V (2.2 nm) may partially neutralize the stronger Nafion®-support interaction and reduce the spillover of the Nafion® hydrophobic component onto the Pt particles. In consequence, the inhibition of ORR is not significantly stronger for Pt4.8G compared to that for Pt4.8V.

The self-assembly of Nafion® around carbon supported catalyst particles and the formation of micelle-like structures with hydrophobic core and hydrophilic shell has important consequences for the catalyst activity determinations utilizing rotating disk electrodes. On one hand, the phenomenon helps making high quality, well dispersed inks, which meet the criteria for accurate RRDE experiments.[16] On the other hand, it leads to ORR inhibition and underestimated catalyst

activities. One of the most dangerous features of ORR inhibition by self-assembled Nafion® under RRDE conditions is that it does not manifest itself in Koutecky-Levich analysis, which makes it difficult to detect. Our previous kinetic ORR results obtained for uncomplexed iron tetraphenylporpohyrin are also affected by the phenomenon and the reported effect of the axial coordination of the active center by polyvinylimidazole overestimated.[37] If Nafion® self-assembly takes place during the fabrication of fuel cell catalyst layers, it may also compromise the cell performance. The phenomenon may have most significant effect on the fuel cell performance of the state of the art heat treated ORR catalysts,[7-9] which are structurally related to the transition metal macrocycles studied by us, *i.e.*, their active centers are embedded in strongly hydrophobic, π - electron rich environments. Consequently, their full potential as ORR catalysts probably cannot be realized in fuel cells utilizing Nafion® as the electrolyte.

ACKNOWLEDGEMENT

The authors want to express their gratitude for the financial support from the UC Office of the President (Lab Fees Research Program, grant ID# 12-LR-237440).

REFERENCES

1. Mauritz, K. A.; Moore, R. B., State of Understanding of Nafion. *Chem. Rev.* **2004**, *104*, 4535-4585.

2. Wei, Z. D.; Ran, H. B.; Liu, X. A.; Liu, Y.; Sun, C. X.; Chan, S. H.; Shen, P. K., Numerical Analysis of Pt Utilization in PEMFC Catalyst Layer Using Random Cluster Model. *Electrochim. Acta* **2006**, *51*, 3091-3096.

3. Sasikumar, G.; Ihm, J. W.; Ryu, H., Dependence of Optimum Nafion Content in Catalyst Layer on Platinum Loading. *J. Power Sources* **2004**, *132*, 11-17.

4. Wagner, N.; Kaz, T.; Friedrich, K. A., Investigation of Electrode Composition of Polymer Fuel Cells by Electrochemical Impedance Spectroscopy. *Electrochim. Acta* **2008**, *53*, 7475-7482.

5. Lee, M.; Uchida, M.; Yano, H.; Tryk, D. A.; Uchida, H.; Watanabe, M., New Evaluation Method for the Effectiveness of Platinum/Carbon Electrocatalysts under Operating Conditions. *Electrochim. Acta* **2010**, *55*, 8504-8512.

6. Curnick, O. J.; Pollet, B. G.; Mendes, P. M., Nafion1-Stabilised Pt/C Electrocatalysts with Efficient Catalyst Layer Ionomer Distribution for Proton Exchange Membrane Fuel Cells. *RSC Adv.* **2012**, *2*, 8368-8374.

7. Wang, B., Recent Development of Non-Platinum Catalysts for Oxygen Reduction Reaction. *J. Power Sources* **2005**, *152*, 1-15.

8. Othman, R.; Dicks, A. L.; Zhu, Z., Non Precious Metal Catalysts for the Pem Fuel Cell Cathode. *Int. J. Hydrogen Energy* **2012**, *37*, 357-372.

9. Chen, Z.; Higgins, D.; Yu, A.; Zhang, L.; Zhang, J., A Review on Non-Precious Metal Electrocatalysts for Pem Fuel Cells. *Energy Environ. Sci.* **2011**, *4*, 3167-3192.

10. Morozan, A.; Campidelli, S.; Filoramo, A.; Jousselme, B.; Palacin, S., Catalytic Activity of Cobalt and Iron Phthalocyanines or Porphyrins Supported on Different Carbon Nanotubes Towards Oxygen Reduction Reaction. *Carbon* **2011**, *49*, 4839-4847.

11. Fukuzumi, S.; Yamada, Y.; Karlin, K. D., Hydrogen Peroxide as a Sustainable Energy Carrier: Electrocatalytic Production of Hydrogen Peroxide and the Fuel Cell. *Electrochim. Acta* **2012**, *82*, 493-511.

12. Saveant, J.-M., Molecular Catalysis of Electrochemical Reactions. Mechanistic Aspects. *Chem. Rev.* **2008**, *108*, 2348-2378.

13. Zagal, J. H., Metallophthalocyanines as Catalysts in Electrochemical Reactions. *Coord. Chem. Rev.* **1992**, *119*, 89-136.

14. Rosenthal, J.; Nocera, D. G., Role of Proton-Coupled Electron Transfer in O–O Bond Activation. *Acc. Chem. Res.* **2007**, *40*, 543-553.

15. Chlistunoff, J., RRDE and Voltammetric Study of ORR on Pyrolyzed Fe/Polyaniline Catalyst. On the Origins of Variable Tafel Slopes. *J. Phys. Chem. C* **2011**, *115*, 6496-6507.

16. Garsany, Y.; Baturina, O. A.; Swider-Lyons, K. E.; Kocha, S. S., Experimental Methods for Quantifying Electrocatalysts for the Oxygen Reduction Reaction. *Anal. Chem.* **2010**, *82*, 6321-6328.

17. Durst, J.; Siebel, A.; Simon, C.; Hashe, F.; Herranz, J.; Gasteiger, H. A., New Insights into the Electrochemical Hydrogen Oxidation and Evolution Reaction Mechanism. *Energy Environ. Sci.* **2014**, *7*, 2255-2260.

18. Durst, J.; Simon, C.; Hashe, F.; Gasteiger, H. A., Hydrogen Oxidation and Evolution Reaction Kinetics on Carbon Supported Pt, Ir, Rh, and Pd Electrocatalysts in Acidic Media. *J. Electrochem. Soc.* **2015**, *162*, F190-F203.

19. Kinoshita, K., *Carbon: Electrochemical and Physicochemical Properties*; John Wiley & Sons: New York, NY, 1988.

20. Hashe, F.; Oezaslan, M.; Strasser, P., Activity, Stability and Degradation of Multi Walled Carbon Nanotube (MWCNT) Supported Pt Fuel Cell Electrocatalysts. *Phys. Chem. Chem. Phys.* **2010**, *12*, 15251-15258.

21. Guzman-Blas, R.; Suazo-Davila, D.; Velez, C. A.; Daza, C. E.; Stacchiola, D. J.; Sasaki, K.; Senanayake, S. D.; Johnston-Peck, A. C.; Molina, R.; Cabrera, C. R., Edta-Ce(III) Modified Pt Vulcan XC-72 Catalyst Synthesis for Methanol Oxidation in Acid Solution. *Electrocatalysis* **2014**, *5*, 50-61.

22. Scherrer, P., Bestimmung Der Grösse Und Der Inneren Struktur Von Kolloidteilchen Mittels Röntgenstrahlen. *Nachrichten von der Gesellschaft der Wissenschaften, Göttingen* **1918**, 98-100.

23. Langmuir, I., The Adsorption of Gases on Plane Surfaces of Glass, Mica and Platinum. *J. Am. Chem. Soc.* **1918**, *40*, 1361-1403.

24. Paul, D. K.; Karan, K.; Docoslis, A.; Giorgi, J. B.; Pearce, J., Characteristics of Self-Assembled Ultrathin Nafion Films. *Macromolecules* **2013**, *46*, 3461-3475.

25. Castanheira, L.; Silva, W. O.; Lima, F. H. B.; Crisci, A.; Dubau, L.; Maillard, F., Carbon Corrosion in Proton-Exchange Membrane Fuel Cells: Effect of the Carbon Structure, the Degradation Protocol, and the Gas Atmosphere. *ACS Catal.* **2015**, *5*, 2184-2194.

26. Artyushkova, K.; Pylypenko, S.; Dowlapalli, M.; Atanassov, P., Structure-to-Property Relationships in Fuel Cell Catalyst Supports:Correlation of Surface Chemistry and Morphology with Oxidation Resistance of Carbon Blacks. *J. Power Sources* **2012**, *214*, 303-313.

27. Masuda, T.; Naohara, H.; Takakusagi, S.; Singh, P. R.; Uosaki, K., Formation and Structure of Perfluorosulfonated Ionomer Thin Film on a Graphite Surface. *Chem. Lett.* **2009**, *38*, 884-885.

28. Harris, P. J. F., Fullerene-Related Structure of Commercial Glassy Carbons. *Phil. Mag.* **2004**, *84*, 3159-3167.

29. Bard, A. J.; Faulkner, L. R., *Electrochemical Methods: Fundamentals and Applications.*, 2nd ed.; John Wiley & Sons: New York, Chichester, Weinheim, Brisbane, Singapore, Toronto, 2001, p 833.

30. Jiang, P.; Ma, X.; Ning, J.; Song, C.; Chen, X.; Jia, J.-F.; Xue, Q.-K., Quantum Size Effect Directed Selective Self-Assembling of Cobalt Phthalocyanine on Pb(111) Thin Films. *J. Am. Chem. Soc.* **2008**, *130*, 7790-7791.

31. Kozub, B. R.; Compton, R. G., Voltammetric Studies of the Redox Mediator, Cobalt Phthalocyanine, with Regard to Its Claimed Electrocatalytic Properties. *Sensors and Actuators B* **2010**, *147*, 350-358.

32. Damjanovic, A.; Brusic, V., Electrode Kinetics of Oxygen Reduction on Oxide-Free Platinum Electrodes. *Electrochim. Acta* **1967**, *12*, 615-628.

33. Mashio, T.; Malek, K.; Eikerling, M.; Ohma, A.; Kanesaka, H.; Shinohara, K., Molecular Dynamics Study of Ionomer and Water Adsorption at Carbon Support Materials. *J. Phys. Chem. C* **2010**, *114*, 13739-13745.

34. Soboleva, T.; Zhao, X.; Malek, K.; Xie, Z.; Navessin, T.; Holdcroft, S., On the Micro-, Meso-, and Macroporous Structures of Polymer Electrolyte Membrane Fuel Cell Catalyst Layers. *ACS Applied Materials & Interfaces* **2010**, *2*, 375-384.

35. Chlistunoff, J.; Pivovar, B., Effects of Ionomer Morphology on Oxygen Reduction on Pt. *J. Electrochem. Soc.* **2015**, *162*, F890-F900.

36. Freger, V., Hydration of Ionomers and Schroeder's Paradox in Nafion. *J. Phys. Chem. B* **2009**, *113*, 24-36.

37. Chlistunoff, J.; Sansiñena, J.-M., Effects of Axial Coordination of the Metal Center on the Activity of Iron Tetraphenylporphyrin as a Nonprecious Catalyst for Oxygen Reduction. *J. Phys. Chem. C* **2014**, *118*, 19139-19149.

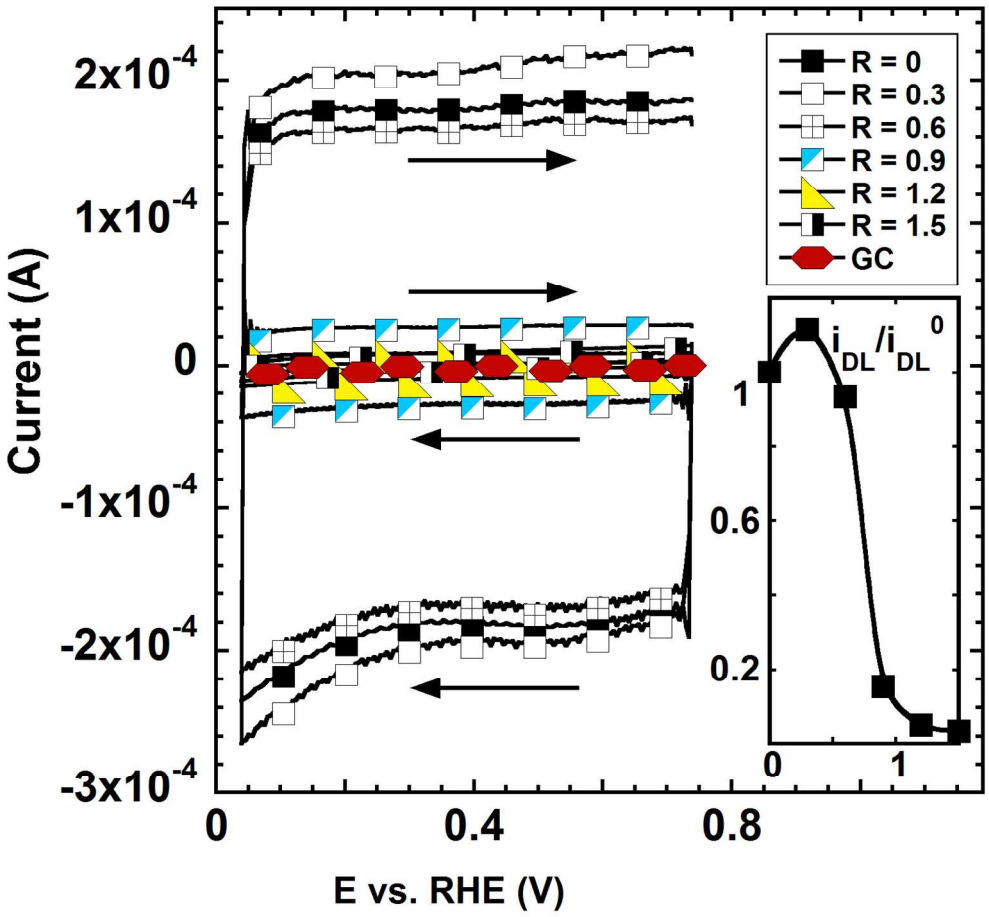

Capacitive voltammetric currents measured for 0.1 mg of Vulcan XC72 mixed with various quantities of 5% Nafion® solution. Scan rate 100 mV s 1. R is the ratio of the volume of 5% Nafion® (µl) to the mass of carbon (mg) used to make the carbon inks. The ratio of the capacitive currents at 0.3 V for various Nafion® contents to that measured in absence of Nafion® is plotted against R in the inset. The currents used to create the graph in the inset were averages of the absolute currents measured at 0.3 V in both forward and reverse scans.
192x189mm (216 x 216 DPI)

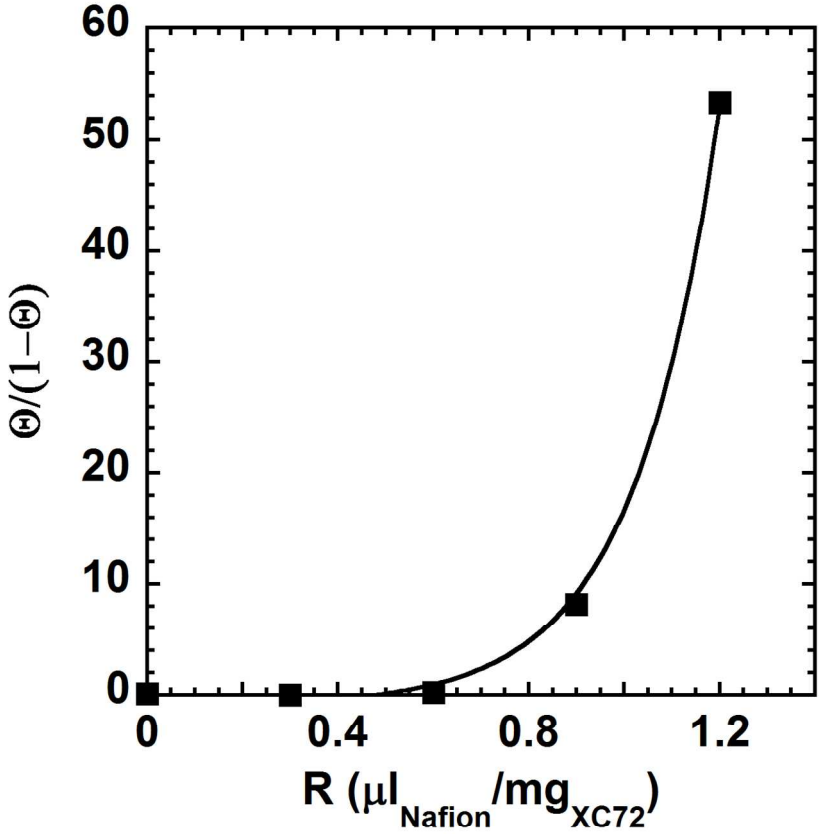

Calculated (eq. 1) ratio of surface areas of Vulcan XC72 covered with Nafion® and not covered plotted versus Nafion® content (R) in the ink.
190x190mm (216 x 216 DPI)

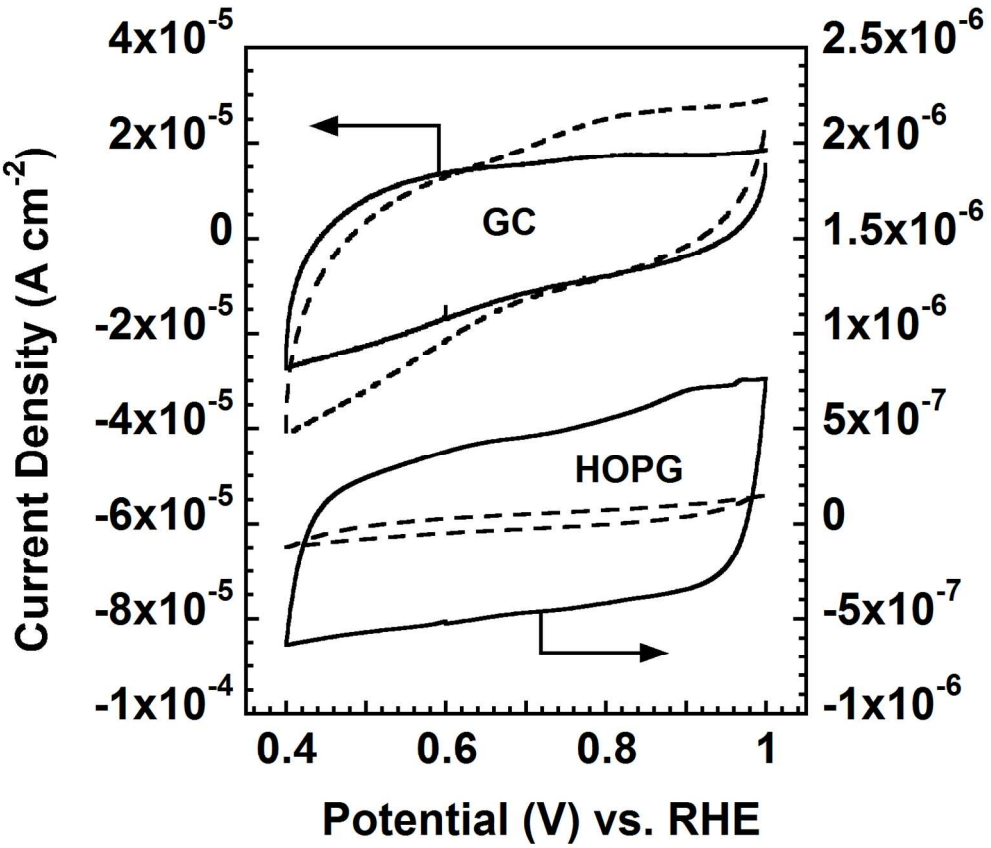

Capacitive voltammetric current densities measured for a 3 mm glassy carbon disk and a 4.8 mm HOPG electrode in 0.5 mol dm^{-3} sulfuric acid before (solid lines) and after depositing Nafion® film (see text).
190x190mm (216 x 216 DPI)

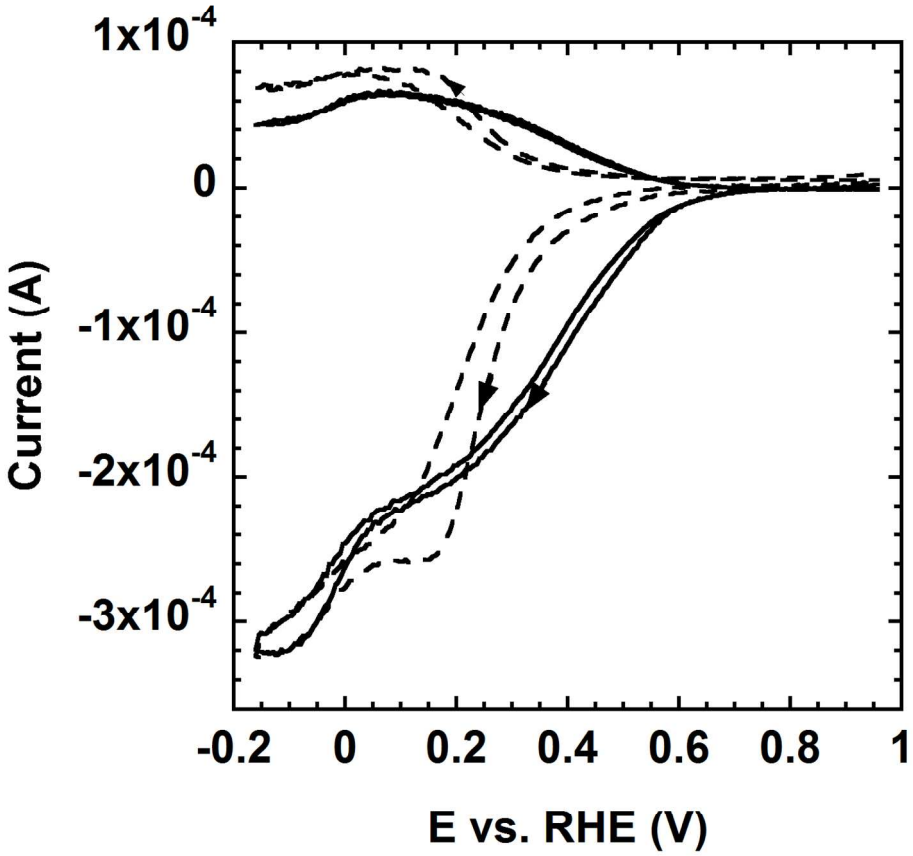

Background corrected RRDE currents for ORR (disk – negative, ring – positive) recorded for 7.5% CoPC supported on Vulcan XC72 and two Nafion® contents. R = 0.3 - solid lines, R = 1.2 – dashed lines. Total carbon loading 0.1 mg. Rotation rate 400 rpm. Scan rate 10 mV s^{-1}.
190x190mm (216 x 216 DPI)

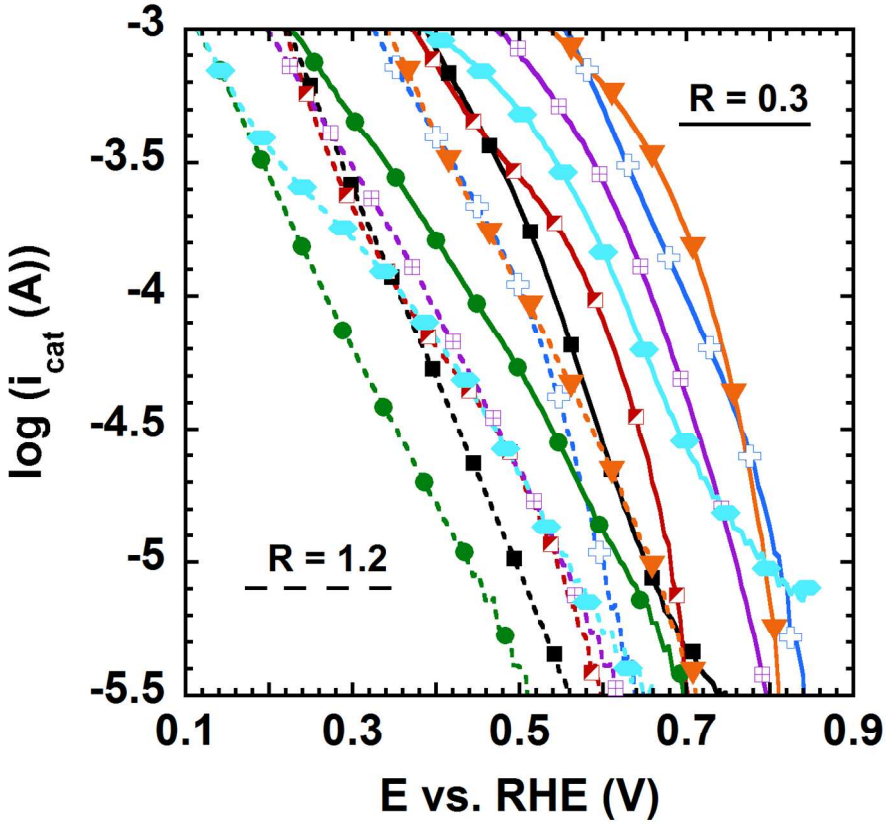

Kinetic ORR currents determined from first reverse (anodic) scans of RRDE voltammograms measured for Co and Fe porphyrins and phtalocyanines supported on Vulcan XC72. Nafion® content (R): 0.3 – solid lines, 1.2 – dashed lines. Total Vulcan XC72 loading 0.1 mg. Rotation rate 400 rpm. Scan rate 10 mV s^{-1}. Weight percentage of the complexes in the catalysts (excluding Nafion®): FeOEPCl – 8.1 (full black squares); FeTPPCl – 9.0 (half filled red squares); CoOEP – 7.6 (blue crosses); CoPC – 7.5 (full green circles); CoTPP – 8.6 (purple crossed squares); CoTMeOPP – 6.2 (orange triangles); FePCCl – 7.9 (light blue hexagons). 190x190mm (216 x 216 DPI)

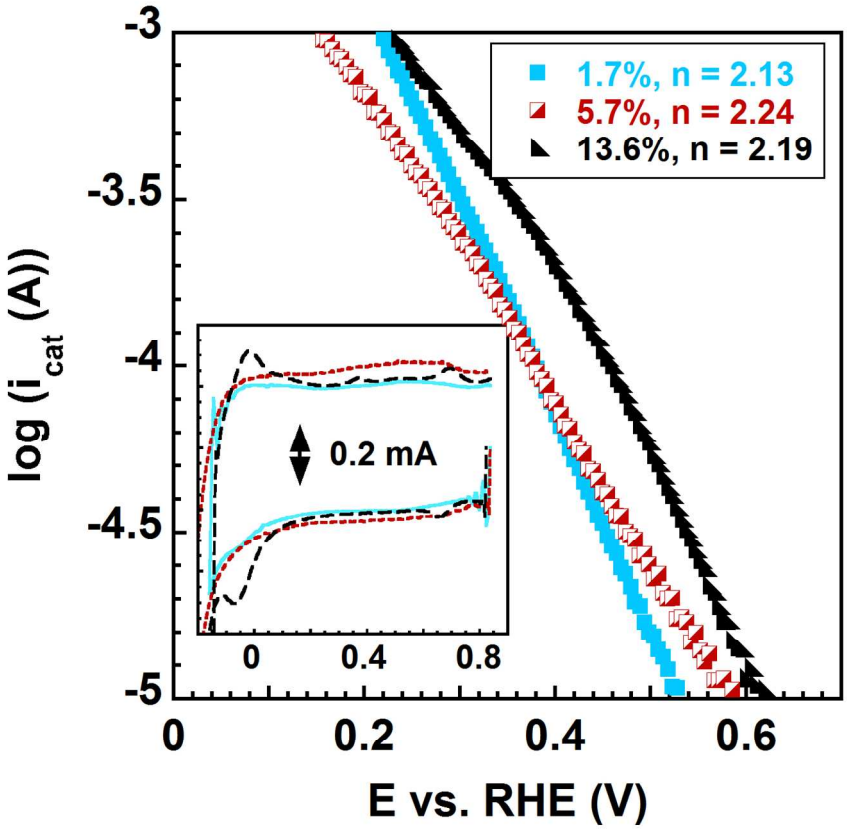

Kinetic ORR currents determined from first reverse (anodic) scans of RRDE voltammograms measured for various quantities of CoPC supported on Vulcan XC72. R = 0.6. Total carbon loading 0.1 mg. CoPC contents (weight %) listed in the legend. Rotation rate 400 rpm. Scan rate 10 mV s^{-1}. Inset: cyclic voltammograms recorded for the catalysts in absence of oxygen at 100 mV s^{-1}. CoPC contents (weight %): 1.7 – solid blue line; 5.7 – short dashed red line, 13.6 – long dashed black line. Reduction and oxidation peaks corresponding to CoPC are clearly visible only for the 13.6% CoPC (long dashed black line).
190x190mm (216 x 216 DPI)

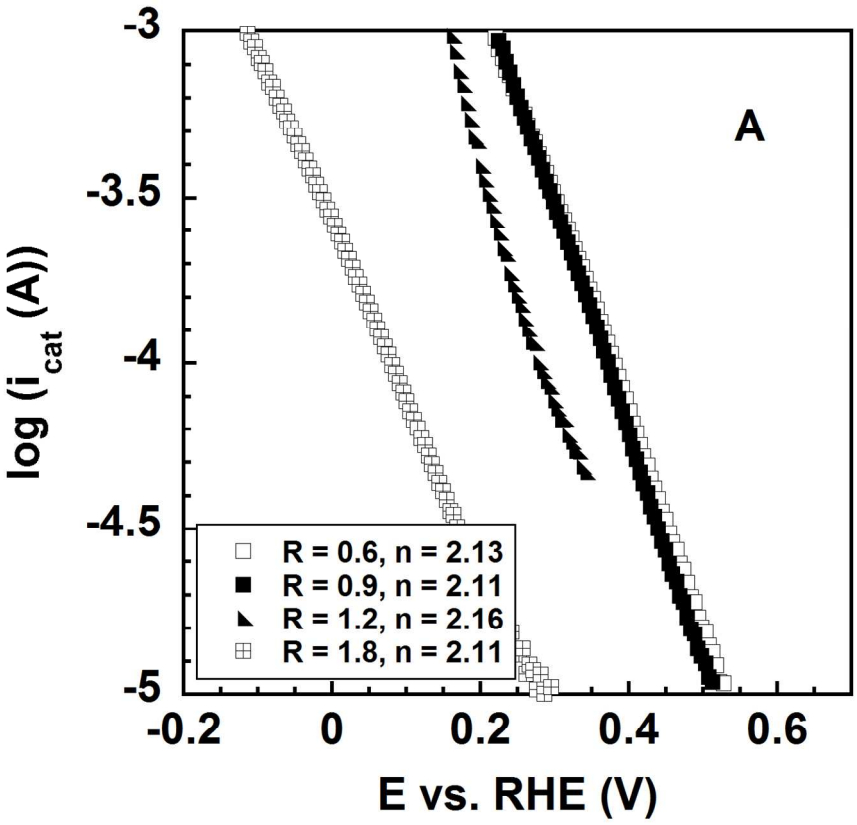

Effects of Nafion® on the kinetic ORR currents for catalysts containing three different quantities of CoPC: 1.7% (A); 5.7% (B); 13.6% (C). Total Vulcan XC72 loading 0.1 mg. Rotation rate 400 rpm. Scan rate 10 mV s^{-1}. Nafion contents (R) and average number of electrons transferred in ORR (n) listed in the legend.
190x190mm (216 x 216 DPI)

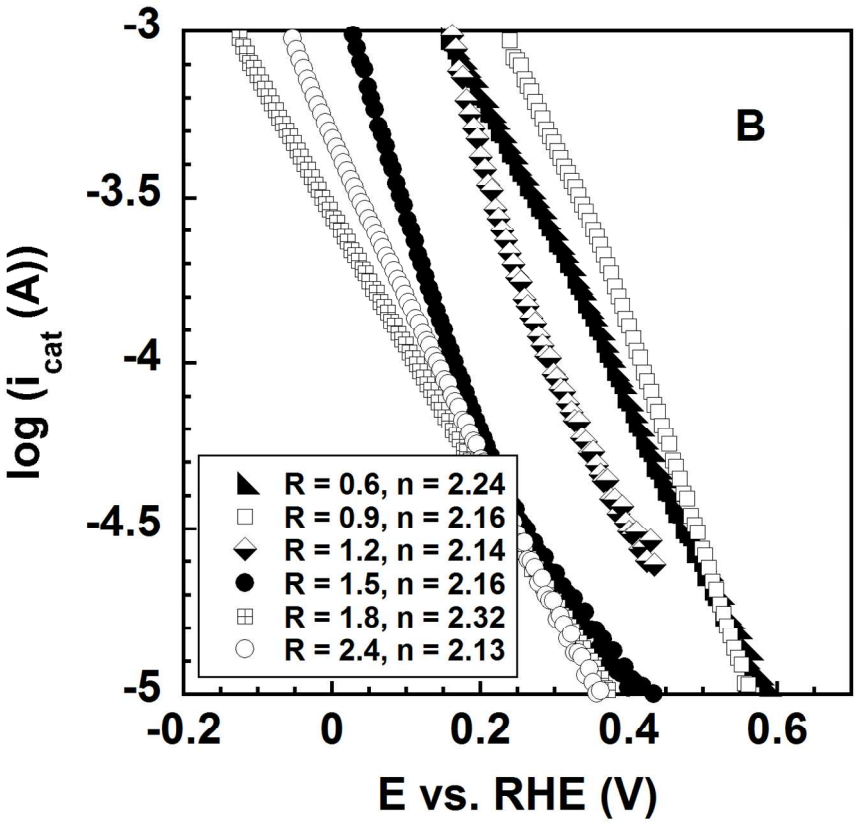

Effects of Nafion® on the kinetic ORR currents for catalysts containing three different quantities of CoPC: 1.7% (A); 5.7% (B); 13.6% (C). Total Vulcan XC72 loading 0.1 mg. Rotation rate 400 rpm. Scan rate 10 mV s^{-1}. Nafion contents (R) and average number of electrons transferred in ORR (n) listed in the legend.
190x190mm (216 x 216 DPI)

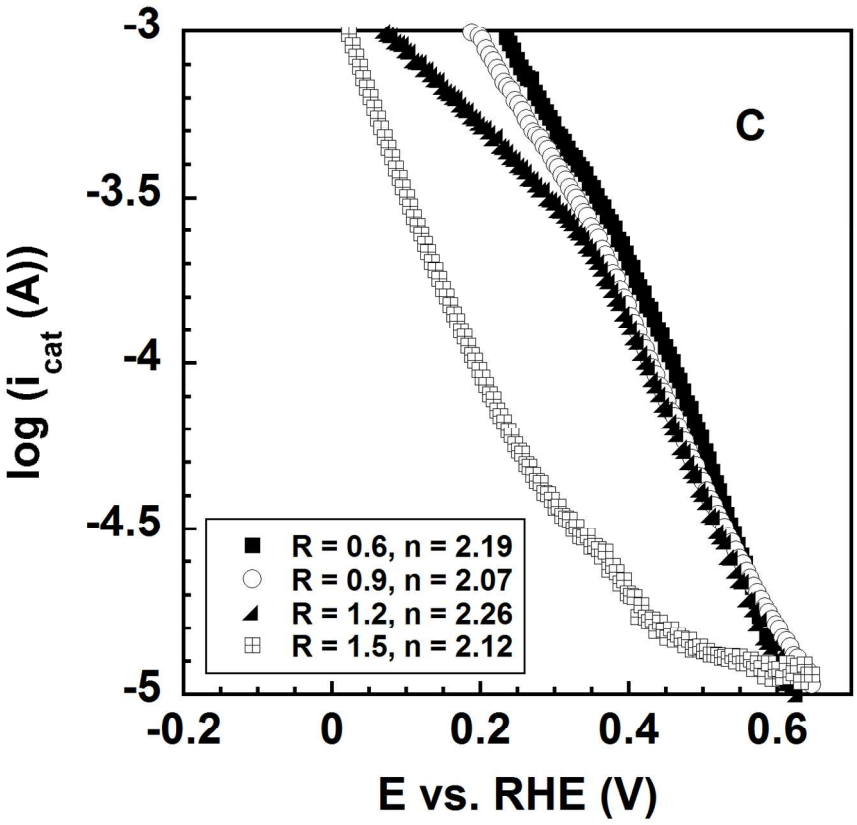

Effects of Nafion® on the kinetic ORR currents for catalysts containing three different quantities of CoPC: 1.7% (A); 5.7% (B); 13.6% (C). Total Vulcan XC72 loading 0.1 mg. Rotation rate 400 rpm. Scan rate 10 mV s^{-1}. Nafion contents (R) and average number of electrons transferred in ORR (n) listed in the legend.
190x190mm (216 x 216 DPI)

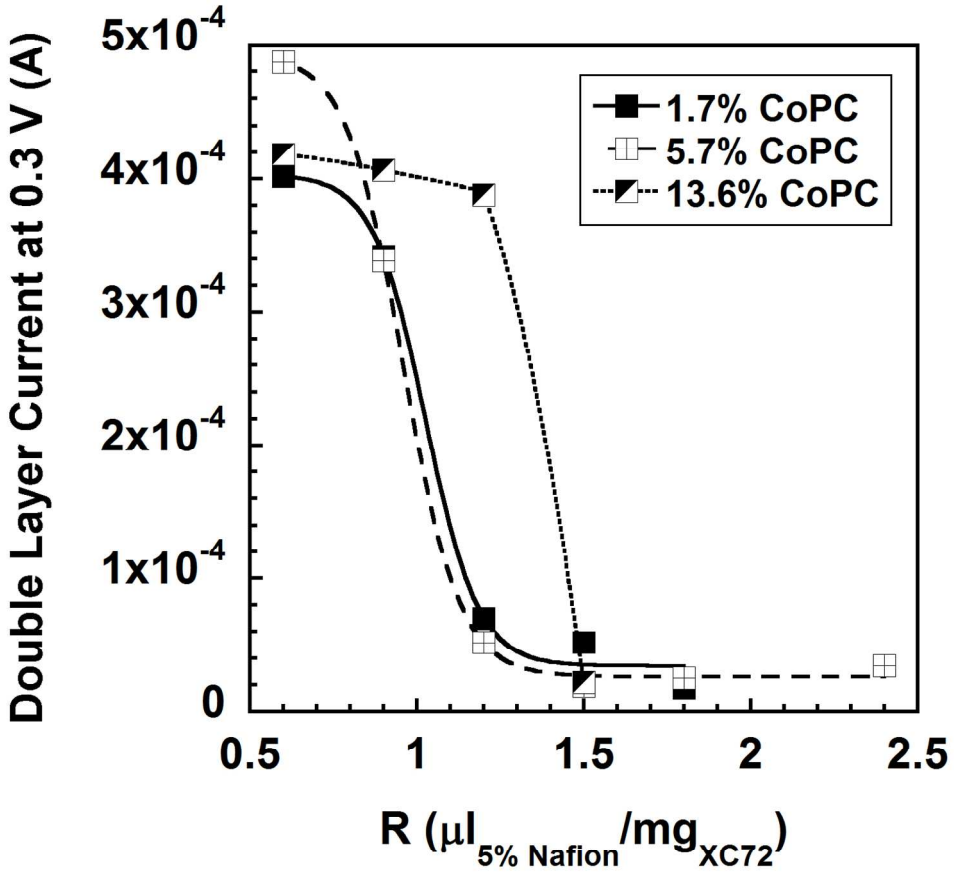

Capacitive currents at 0.3 V for three CoPC + XC72 catalysts plotted against the Nafion® content (R) in the ink. The values plotted are sums of the absolute currents measured in both forward and reverse voltammetric scans recorded at a scan rate of 100 mV s^{-1}. Total Vulcan XC72 loading 0.1 mg.
190x190mm (216 x 216 DPI)

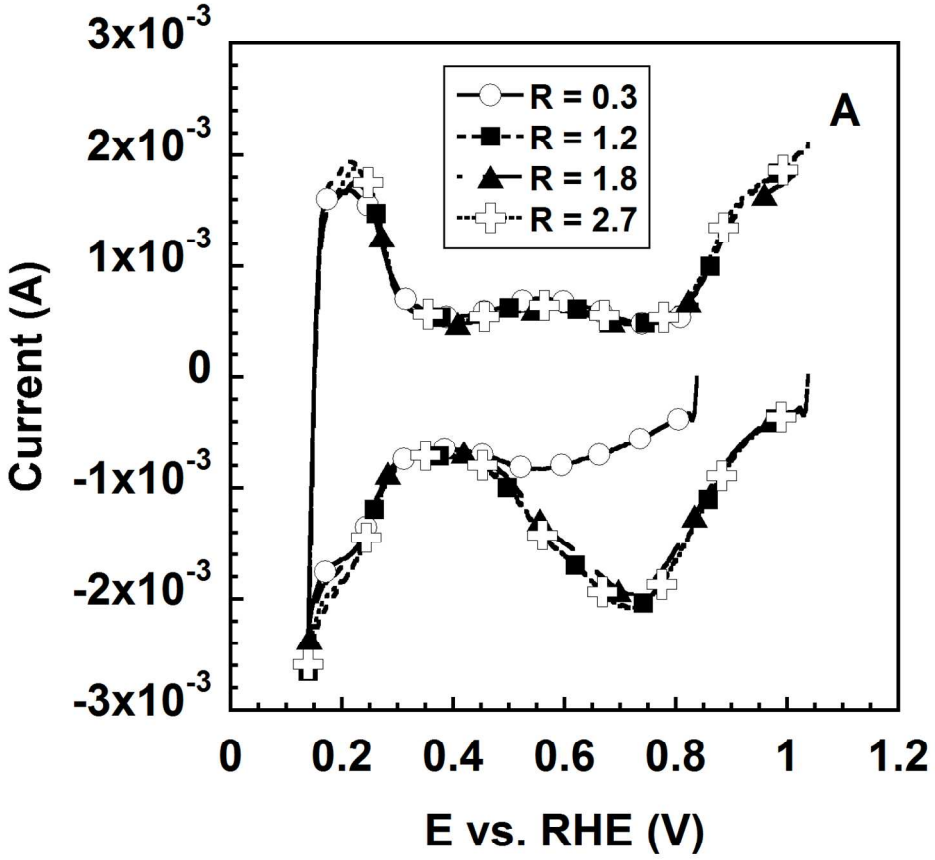

Background currents (A) and ORR kinetic currents (B) measured for Pt20V (0.1 mg total carbon loading) containing various Nafion® quantities (R). Scan rate: 100 mV s^{-1} (A); 10 mV s^{-1} (B). Rotation rate (B): 400 rpm. Scan directions (B) indicated by the arrows parallel to the Tafel plots.
190x190mm (216 x 216 DPI)

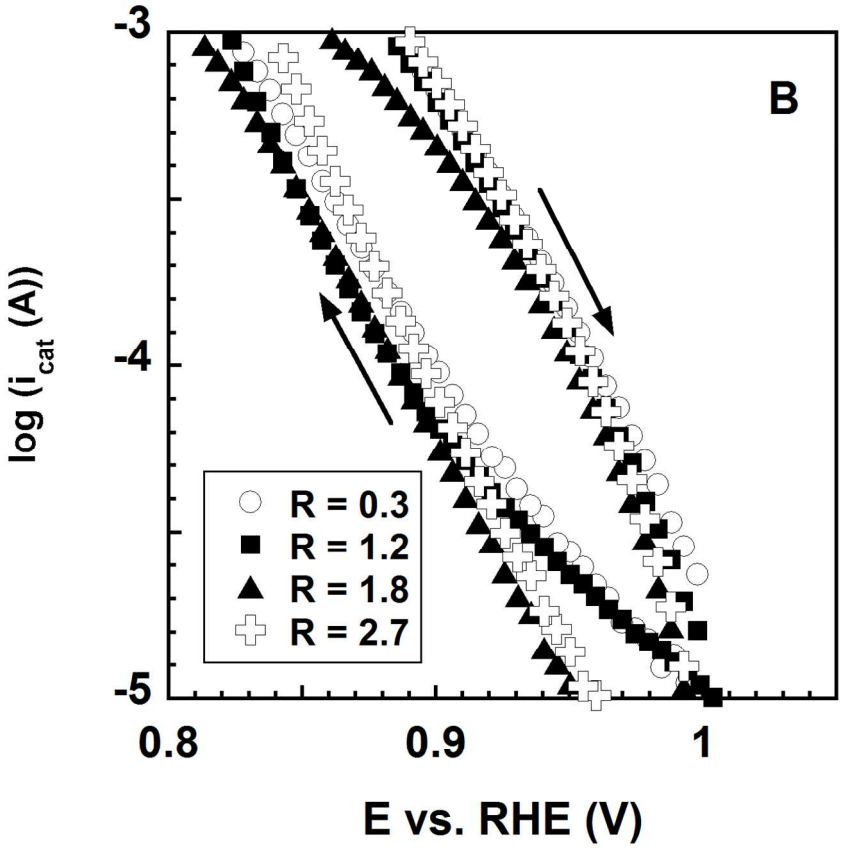

Background currents (A) and ORR kinetic currents (B) measured for Pt20V (0.1 mg total carbon loading) containing various Nafion® quantities (R). Scan rate: 100 mV s^{-1} (A); 10 mV s^{-1} (B). Rotation rate (B): 400 rpm. Scan directions (B) indicated by the arrows parallel to the Tafel plots.
190x190mm (216 x 216 DPI)

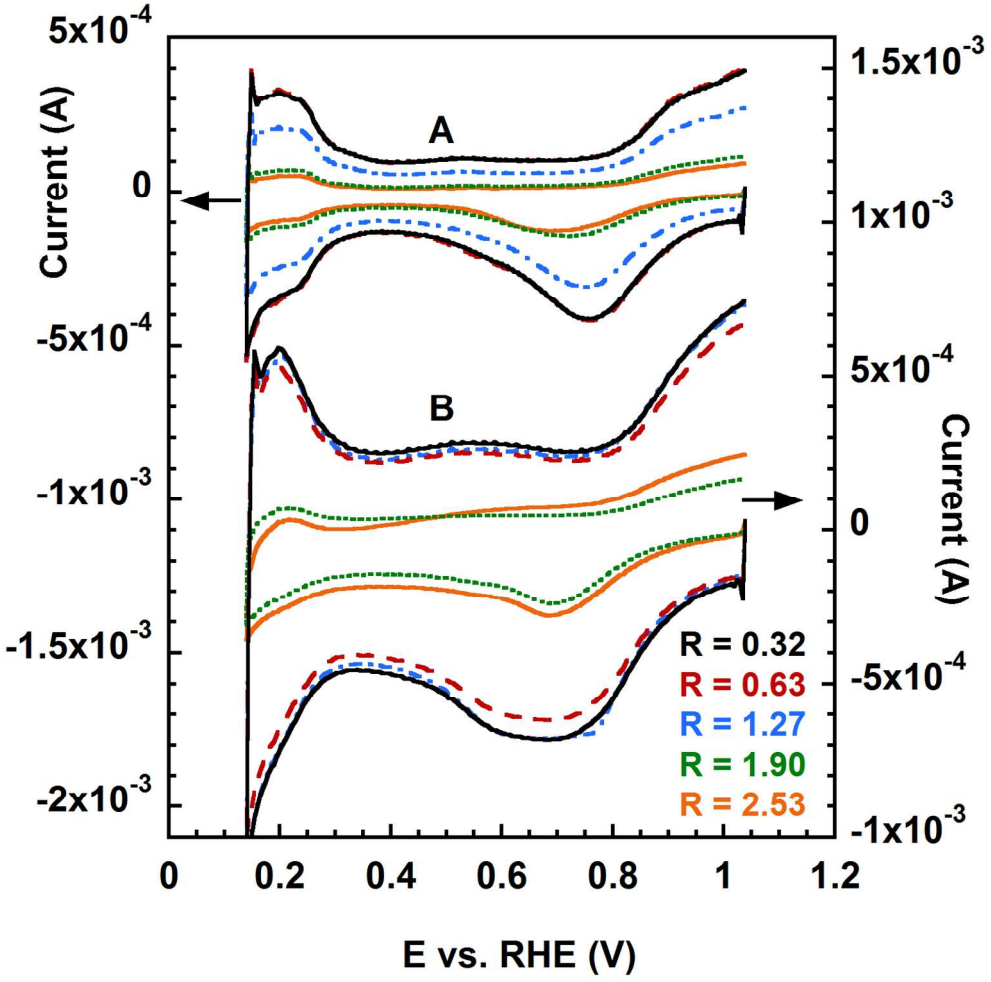

Background currents measured for Pt4.8G (A) and Pt4.8V (B) catalysts containing various quantities (R) of Nafion®. Scan rate 100 mV s^{-1}. Total carbon support loading 0.1 mg.
190x190mm (216 x 216 DPI)

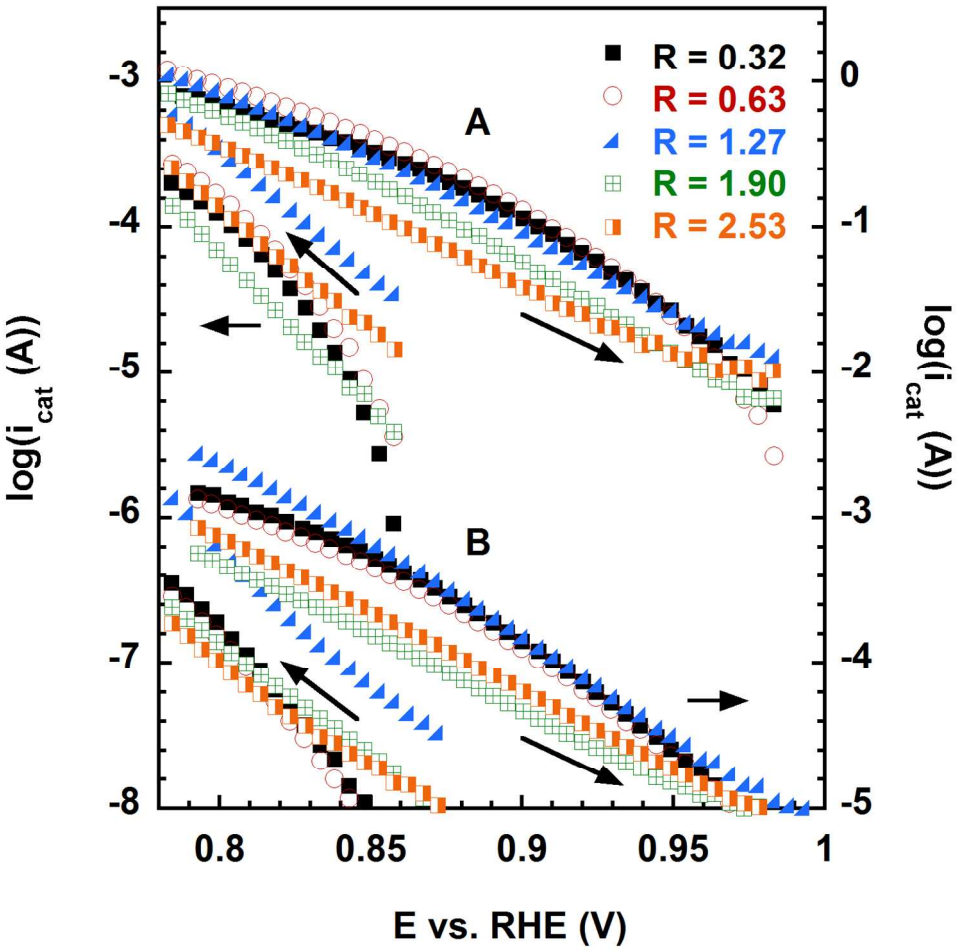

ORR kinetic currents measured for Pt4.8G (A) and Pt4.8V (B) catalysts containing various quantities (R) of Nafion®. Scan rate 10 mV s^{-1}. Rotation rate 400 rpm. Scan directions indicated by the arrows parallel to the Tafel plots.
190x190mm (216 x 216 DPI)

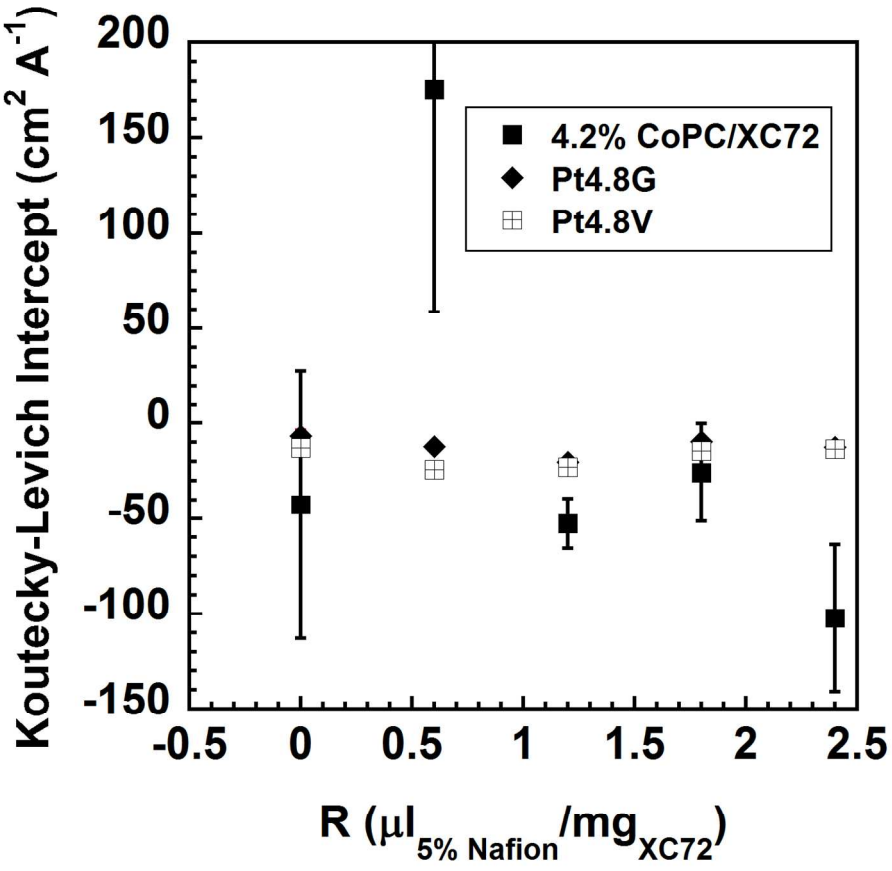

Intercepts of the Koutecky Levich plots for the limiting ORR currents in O2 saturated solutions measured from experiments performed at 400, 625, 900, 1225, 1600, 2025 and 2500 rpm rotation rates. The error bars reflect the respective errors of the intercepts obtained from the linear fitting and are too short to be seen for the Pt catalysts.
190x190mm (216 x 216 DPI)

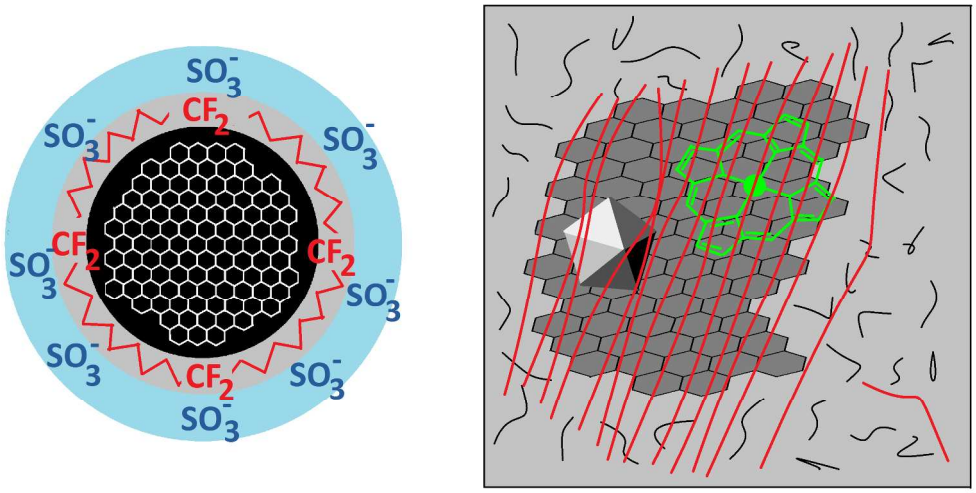

Table of content
775x393mm (96 x 96 DPI)